DISTANCE OPTIMISATION FOR A LINEAR ARRANGEMENT OF VERTICAL AXIS WIND TURBINES

Fajer Mohamed

Master of Science by Research

2017

University of Huddersfield

School of Computing and Engineering

DECLARATION

i. The author of this thesis (including any appendices and/or schedules to this thesis) owns any copyright in it (the "Copyright") and she has given The University of Huddersfield the right to use such copyright for any administrative, promotional, educational and/or teaching purposes.

ii. Copies of this thesis, either in full or in extracts, may be made only in accordance with the regulations of the University Library. Details of these regulations may be obtained from the Librarian. This page must form part of any such copies made.

iii. The ownership of any patents, designs, trademarks and any and all other intellectual property rights except for the Copyright (the "Intellectual Property Rights") and any reproductions of copyright works, for example graphs and tables ("Reproductions"), which may be described in this thesis, may not be owned by the author and may be owned by third parties. Such Intellectual Property Rights and Reproductions cannot and must not be made available for use without the prior written permission of the owner(s) of the relevant Intellectual Property Rights and/or Reproductions.

ACKNOWLEDGEMENTS

Firstly, I would like to thank Allah for every step in my life. I want to thank my mother and father for their continuous support and encouragement throughout my life.

I would like to acknowledge my sincerest gratitude to my supervisors Prof. John Chai and Dr Viacheslav Stetsyuk who supported me throughout my research. I would also like to thank Prof. Ian Glover for his support and advice during this research.

And finally, I would like to express my sincere gratefulness to the University of Huddersfield for giving me this great opportunity to work on this project and for all the motivation, support and encouragement.

ABSTRACT

For many centuries, researchers and scholars have been effortlessly trying to harvest natural energy resources, such as wind energy, solar energy and geothermal energy, due to the diminution of fossil fuels and their harmful effects on the surrounding environment. The wind has been shown to possess an incredible amount of power, which can be harnessed using wind turbines. Wind turbines transform the kinetic energy available in the free stream wind into mechanical energy by a rotor, from which power can be generated.

Wind turbines can be broadly classified into two main categories, depending on the orientation of their axis of rotation; Horizontal Axis Wind Turbines (HAWT) and Vertical Axis Wind Turbines (VAWT). VAWTs are more suitable for the urban environment due to their low start-up torque.

Extensive research has been carried out in improving the design and performance of a VAWT. However, a number of key issues have been highlighted after conducting an extensive literature; these key issues form the scope of this research.

The current study focuses on optimising the distance between VAWT's placed side by side linearly, by analysing the flow around a single VAWT using advanced numerical modelling tools. This study is carried out by analysing the wake region formed by the flow field under various free stream wind velocities. Furthermore, maximum wake region will be identified to measure the maximum distance the free stream wind velocity can occupy in the VAWT vicinity.

Finally, a novel mathematical model that predicts the optimal distance required to place a side by side VAWT under various flow conditions will be developed. It is expected that this study will be able to optimise the spacing between VAWTs in a wind farm.

CONTENTS

LIST OF FIGURES

LIST OF TABLES

NOMENCLATURE

A	Wind turbine inlet area [m^2]
C_P	Wind turbine power coefficient
C_T	Wind turbine torque coefficient
D	Diameter of Wind Turbine [m]
H	Height of wind turbine [m]
L	Length [m]
P	Wind Turbine Power Output [W]
p_∞	Free-Stream Static Pressure [Pa]
p	Local Pressure [Pa]
r	Wind turbine radial position [m]
R_{so}	Outer radius of stator
R_{si}	Inner radius of stator
R_{ro}	Outer radius of rotor
R_{ri}	Inner radius of rotor
R_{co}	Outer radius of core
T	Torque [Nm]
T_{TOTAL}	Wind turbine rotor torque output [Nm]
v	Velocity of blade [m/s]
V_{AVG}	Area-weighted average velocity [m/s]
U_∞	Free-stream velocity [m/s]
X	Domain stream-wise length [m]
X_1	Domain turbine offset in X axis [m]
Y	Domain normal to stream-wise length [m]
Y_1	Domain turbine offset in Y axis [m]
Z	Domain height [m]
Z_1	Domain height offset in Z axis [m]

GREEK SYMBOLS

ρ	Air Density [kg/m^3]
μ	Dynamic Air Viscosity [Pa.S]
α	Guide blade angle [˚]
λ	Rotor blade tip speed ratio
ω	Rotor angular velocity [rad/s]

Chapter 1
Introduction

This chapter provides a synopsis of the current wind power technology used and developed over the years and the importance of wind energy in our present lives. It also provides a detailed review of the types of wind turbines available in the current market used to harness wind energy, HAWT and VAWT. This study focuses on the vertical axis wind turbine (VAWT) due to its advantages that are omnidirectional and easy installation. This chapter reviews the research aim of this study and the motivation that has led us to undertake this research.

1.1. WIND POWER

Wind is a source of renewable energy and is a result of the uneven heating of the atmosphere by the sun. Humans have been harnessing wind energy for over a thousand years, starting in Persia in the nineth century when the traditional windmill was used as a source of energy to do the job of nearly 200 men. [1]

Figure 1: Traditional Windmill Persia [2]

In the 1920's a French man named George Darrieus introduced the first vertical axis wind turbine (The Eggbeater). Sigurd Johannes Savonius (1922) introduced drag based VAWT named the Savonius wind turbine. In the 1930's, eight million HAWT's were installed in England and Holland, and in the early 1950s, a German constructor installed the first wind power plant for mass production. Furthermore, in 1956 Poul la Cour a former student from Denmark constructed a three-bladed wind turbine called 'the Gedser'. [3] [1]

Figure 2: The Gedser [3]

In Canada, South and Rangi (1960-1975) developed and tested the Eggbeater windmill design that was initially introduced by George Darrieus. The Eggbeater windmill showed 30% increase in efficiency in comparison to Savonius rotor. [4] [1]

Due to the increase in the price of oil in 1973, researchers have been undertaking excessive research to discover alternate ways of replacing fossil fuels, coal and gas with unlimited natural energy sources. NASA Glen conducted research on thirteen large-scale wind turbines in the 70s in the United States of America. [4] [1]

The first wind farm was built in the 1980s in New Hampshire in the USA, which consisted of twenty turbines. Additionally, in 1981 NASA succeeded in building a 7.5MW Mod-2 turbine in Washington, followed by 3.2MW two-bladed wind turbines Mod-5B in Hawaii. [1]

The first offshore wind farm that consisted of 11,450 kW turbines was constructed in Denmark in 1991. In Denmark, 20% of the power generated from wind energy is developed by universities, which motivates and supports the wind energy industry and aims to reduce the high costs of electricity by using wind turbines. [5] [6] [1]

Wind energy started developing on a mass scale in 1992 when almost all nations signed the climate change agreement in Rio. Great Britain started its development of wind energy at around this time, with production beginning in Cornwall; the first windfarm consisted of ten turbines that produced power for 2700 houses. [1] [7]

In 2003 the first UK offshore wind farm, which consisted of thirty wind turbines, installed in north Wales, and produced 2MW of energy. The UK has increased its production of wind energy up, producing up to 72MW in 2007 with the installation of Braes O'Doune wind farm in Scotland. By 2008 there were 186 operational wind farms in the UK. [8] [1]

In 2012, the American industry added 13 GW of wind power plants, that produced enough energy to power all the homes in the states of California and Washington. The Wind Technology Market Report (2012) states that wind energy department has employed 80,000 Americans with the development of wind power across the country. [9] [1]

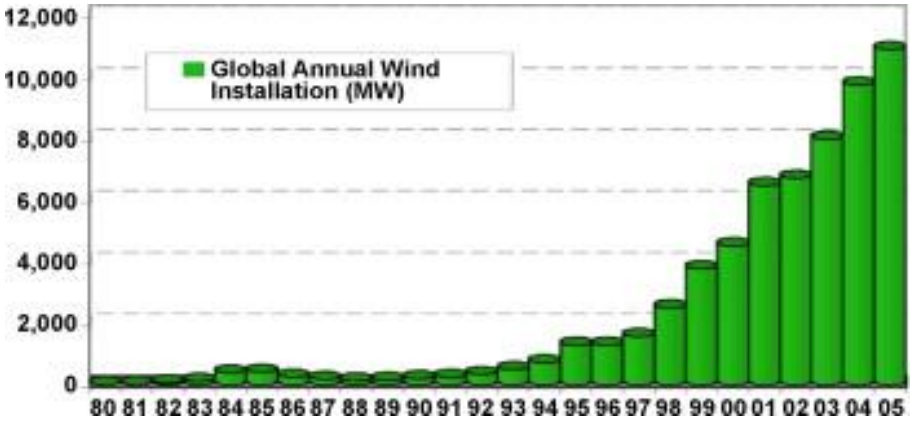

Figure 3: Global annual wind installation from 1980-2005 [10]

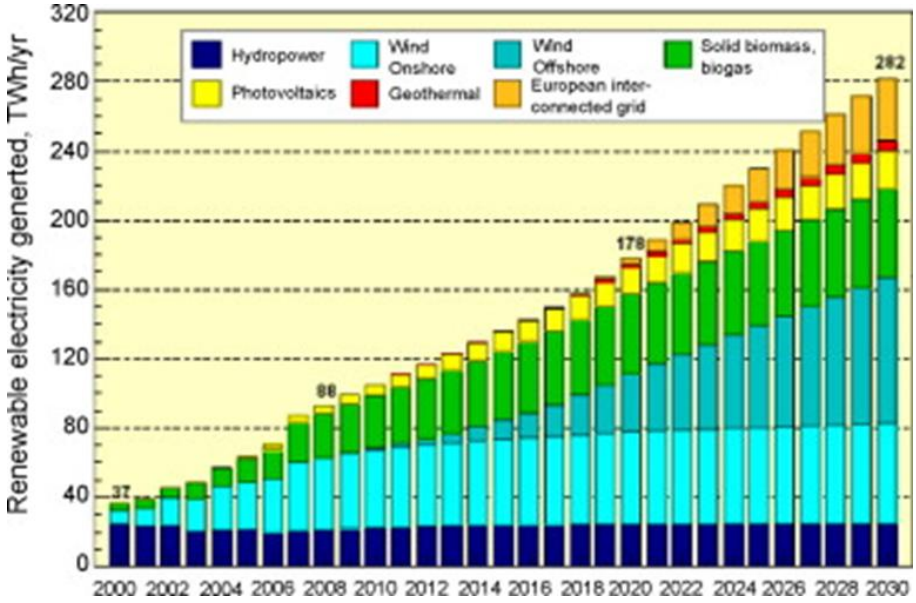

Figure 4: Global annual wind installation plan from 2000 to 2030 [11]

Figure 3 and figure 4 above shows the annual wind installation from 1980 to 2030 where it shows significant rise from the year 2000 onwards. Currently, the UK government targets to increase its production of renewable energy to 20% by 2020, after successfully installing 186 wind farms and 2,120 turbines both offshore and onshore that have the capacity to power 1,523,052 homes. G. M. Joselin Herbert (2007) [12] [1].

Jose Zayas (2014), Director of the Wind and Water Power Technologies Office, states that by reducing electricity costs by 3% will save up to $520 billion between 2014- 2050. [9] [1].

1.2. WIND TURBINES

Wind turbines are the electromechanical systems that transform the kinetic energy available in the wind and convert it to electricity using a generator that is then used for various applications.

1.2.1. Types of wind turbines

Wind turbines are commonly divided into two main categories, determined by the axis of rotation. In Horizontal Axis Wind Turbines (HAWT), the axis of rotation is parallel to the ground whereas Vertical Axis Wind Turbines (VAWT) has an axis of rotation that is normal to the ground.

The horizontal axis wind turbine blades are installed on the main shaft such that the axis of rotation is parallel to the ground. The mechanical control mechanism of the HAWT is installed at the top of the tower, which makes it difficult to reach for maintenance purpose. [1]

On the other hand, the VAWT blades often take the appearance of the Eggbeater like the initial Darrieus wind turbine design. The mechanical components of the turbine generator are mounted at the bottom of the shaft next to the ground. Figure 5 below shows the two types of wind turbines. [1]

Vertical Axis Wind Turbine

Figure 5: Types of Wind Turbines HAWT [13], VAWT [14]

1.3. PERFORMANCE

The most common type of wind turbine in the market is the HAWT, due to its higher performance and efficiency. However, VAWT provides several advantages over HAWT for the urban environment, such as low starting torque, coupled with low noise and self-reliance to the incident flow (omnidirectional). VAWT's require low maintenance and have no limitation on the size of the rotor diameter. This has made VAWT an ideal choice for operation in urban areas. [1]

The most important parameters of a wind turbine, mentioned by Colley [15], is the tip speed ratio (λ), defined as the ratio between the blade angular velocity at its tip and the faraway wind velocity.

$$\lambda = \frac{R\omega}{v} \qquad \text{Equation 1}$$

where ω is the angular velocity of the turbine blade in rad/s, R is the rotor radius in meters and v is the linear wind velocity in m/s.

Moreover, another important parameter to define the vertical axis wind turbine performance is the power defined as work per unit time.

$$P = T.\omega \qquad \text{Equation 2}$$

where T is the torque and ω is the angular velocity, where torque is the force acting on the VAWT that makes it rotate.

The power coefficient is

$$C_p = \frac{P}{\frac{1}{2}\rho U_\infty^3 A} \qquad \text{Equation 3}$$

Where ρ is the density of the air, U_∞ is the free stream velocity and A is the swept area of the rotor.

1.4. TYPES OF VERTICAL AXIS WIND TURBINES

There are two main types of vertical axis wind turbines, the Savonius and the Darrieus. The Darrieus rotor is the first aerodynamic VAWT developed in France by Georges Darrieus. Sandia National Laboratories then developed it in the 1980's; the design of the turbine consists of a number of curved aerofoils that are mounted on a vertical shaft. The working principle of this type of VAWT depends on creating lift force that produces a positive torque to rotate the shaft, and hence generates electricity. Due to the poor efficiency of the Darrieus rotor known as the Eggbeater due to its design; engineers and scholars have continued to modify the wind

turbine design. Giromill turbines are one of the subtype turbines of Darrieus Wind turbines that have been innovated to enhance design, efficiency and power output. The turbine has straight blades that are attached to a central shaft. The design of the turbine replaced the original type of Darrieus turbine the eggbeater, as it is simple, self-starting and easy to build. [16]

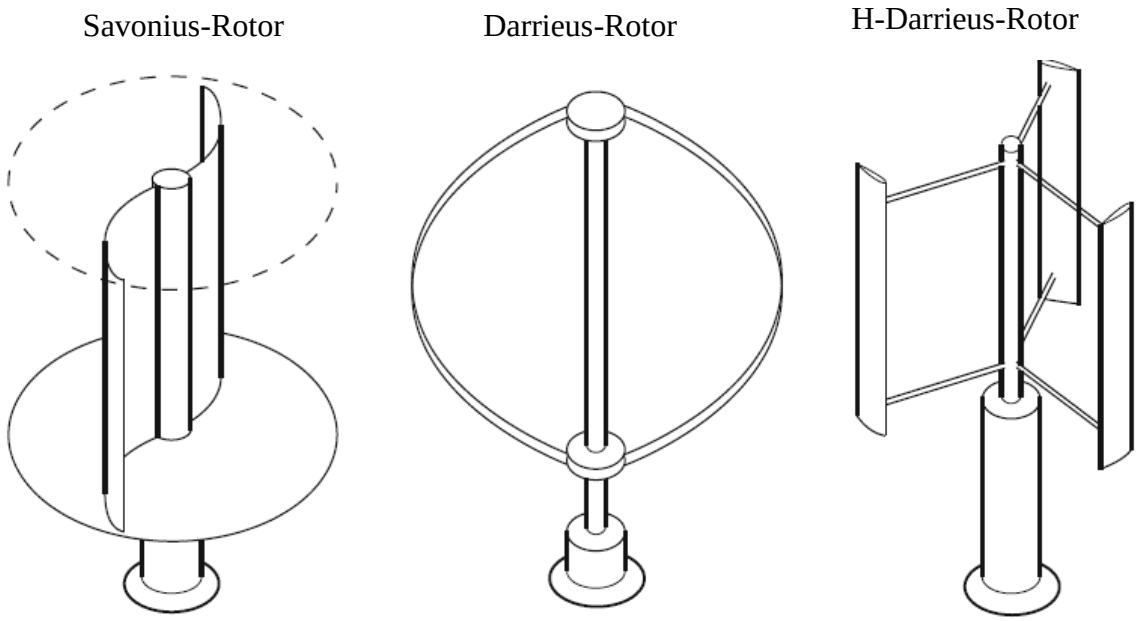

Figure 6: Type of Vertical Axis Wind Turbines [17]

Savonius wind turbines are drag based turbines that consist of a cupped blade (‘S’ shape rotor) that experiences low drag when moving against the wind direction and high drag when moving in the wind direction. The high and low drag causes the wind turbine to rotate. Savonius wind turbines are cost-effective, reliable and can accept the wind from any direction. [1]

1.5. Working Principle of Vertical Axis Wind Turbine

A wind turbine is a device used to extract power from the wind, and convert it to electricity that is then used for different applications. The wind passing over the rotor of a VAWT generates lift, or drag force, that rotates the rotor blades. The rotor is connected to the shaft which in turn is connected to the generator, which then converts the mechanical energy to electricity using a gear drive system. The shaft usually spins at a low speed, and this is connected to a high gear ratio system that results in the optimum speed of the generator shaft, and thereby produces electricity. [18] [1]

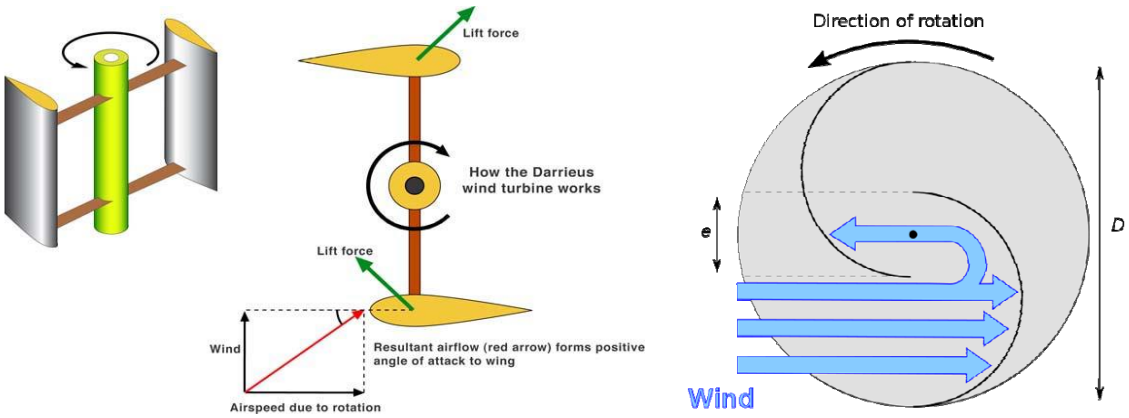

Darrieus Working Principle Savonius Working Principle

Figure 7: Working principle of vertical axis wind turbine [18]

1.6. MOTIVATION

Since the inter-turbine spacing between VAWT's is of essential significance for maximum energy production and minimum wake and turbulence effect in a wind farm. Therefore, a detailed investigation in the wake region is required to determine the inter-turbine spacing for a linear arrangement of VAWT's used in the urban environment.

This study will be conducted using Computational Fluid Dynamics (CFD) analysis to investigate the wake region around a single VAWT under transient flow conditions using a sliding mesh technique to conduct the numerical study. This will provide a better understanding of the wake effects and the distance required to place another VAWT to achieve maximum efficiency and power generation of a number of VAWT placed side by side in an urban area. The current research aims to provide engineers and scholars with an overall idea of the maximum distance required to achieve maximum power generation.

1.7. RESEARCH AIM

Based on the motivation of this research, the research aim of this study is to develop a prediction model that establishes maximum distance required as a function of wind speed for VAWT's. This study will be carried out using ANSYS computational software, where data will further be analysed using CFD post process and MATLAB.

1.8. ORGANISATION OF THESIS

Chapter 1 provides a general review of wind energy and a detailed review of the types of wind turbines in general, and a comprehensive review of the types of vertical axis wind turbines (VAWT) focusing on the Savonius type. It also states the advantages of using vertical axis wind turbines over the horizontal axis wind turbines (HAWT's). In this chapter, the working principle of VAWT has been discussed along with the motivation of this study where the aim of this study has been pointed out.

Chapter 2 consists of a complete literature review of the research that has been conducted by various researchers in the area of wind turbine arrangements in wind farms. A critical review has been carried out on the effect of wake region on the turbine performance, where the scope of the research has been carefully analysed in this section along with the research objectives of this study.

Chapter 3 captures the numerical model prototype design and the fundamental principles of CFD software. It includes modelling of the vertical axis wind turbine, mesh technique, solver setting and the boundary conditions used in this study. It also provides a detailed review of the meshing technique used to mesh the VAWT along with the flow domain. This chapter includes a breakdown hierarchy of the scope of the work that will be conducted in the next chapters.

Chapter 4 comprises of the mesh sensitivity testing and time step size independence testing conducted for 4m/s and 20m/s flow velocity. In addition, vertical axis wind turbine performance under transient wind conditions have been investigated in this chapter along with the flow field analysis. A mathematical prediction tool that is used for distance optimisation for VAWT has been obtained.

Chapter 6 states the research problem synopsis and states the main achievement of this study along with the findings. It clearly mentions that the objectives of this study have been met and further work is recommended for researchers carrying out future work.

Chapter 2
Literature Review

This chapter provides a detailed review of literature in the field concerning wind farms, with emphasis on the various layouts of the vertical axis wind turbines and their importance in improving the overall performance. The main areas addressed in this chapter are related to the flow phenomena around the VAWTs and the form of wake region. Limitations of the existing studies have been identified to determine the scope of this research where objectives of this research have been clearly identified to bridge the gap found in the existing literature.

2.1. INTRODUCTION

The layout scheme of wind farms has been one of the major focuses by researchers and engineers since wind energy became one of the main sources of energy production. From the late 1970's a considerable amount of research has been conducted on the design and development of vertical axis wind turbines (VAWT). A detailed general review of the types and uses of VAWT has been presented in chapter 1 of this thesis. However, the layout scheme of multiple VAWT became one of the main concerns of researchers developing the overall power output in urban areas.

González, J.S., et al. (2014) [19] identified the issues concerning the development of an optimal wind farm arrangement by reviewing the previous work conducted and offering the latest optimization techniques that a designer should consider. The author points out that various factors other than the calculation of the overall energy yield should be considered. Authors such as Cassola, F. (2008), Clarke, A (1989), Ramachandra, T. (2007) and Baban, S.M. (2001) [20] [21] [22] [23] have tackled the issues relating the selection of wind farm location and the various factors that should be considered in selecting the location of the wind farm. Issues such as wake of turbulent wind at the rear area of the vertical axis wind turbine made experts and consult look effectively at the arrangements of the turbine position.

This subdivision of the study starts with a review of the various turbine arrangements and the effect of factors such as optimal distance and wind speed on VAWTS. Numerous computational and experimental studies have been presented here to clearly recognise local flow characteristics around VAWT.

2.2. PERFORMANCE EVALUATION OF VAWT UNDER VARIOUS LAYOUT ARRANGEMENT.

A number of studies have suggested that effective layout arrangements of turbines can enhance power augmentation. Layout case studies have been established by Ying Chen et.al [24] in 2015 to observe the number of wind turbines required in a specified windfarm. The author introduced an advanced wind farm layout technique based on a multi-objective genetic algorithm that specifies the turbine position for both regular and irregular shapes of wind farms. However, the author didn't consider the effect of wake on positioning the wind turbines in the wind farm field and how wake could decrease the overall power generation of the wind farm.

Then Rabia Shakoor et al. [25] in 2015 pointed out that wake calculations are one of the major areas that should be modelled in order to reduce the power loss in the wind farm field. The author examined various wake models and concluded that Jensen's wake model was the best model to solve far wake of wind farms. This study has demonstrated an analysis of the overall wake of a wind farm and has not investigated the wake effect on a single VAWT to solve the layout problem of wind turbines.

In 2016, the wake of a 3D model of a vertical axis wind turbine with two straight blades created using CFD was validated by particle image velocimetry (PIV) test results from existing literature. H.F. Lam and H.Y Peng [26] has defined the far and near wake regions by identifying the velocity defect in the wake region. The author specifies that simulation was based on an inlet velocity of 9.3 m/s and an outlet of zero-gauge pressure. The author points out that the wake downstream requires more time to be developed in comparison to the wake upstream. Figure 8, shows the shape of the completed far wake downstream has been developed after the 29th revolution. This study focuses on one velocity variation, and various velocity variation should be considered for future studies to fully analyse the numerous shapes of wake region.

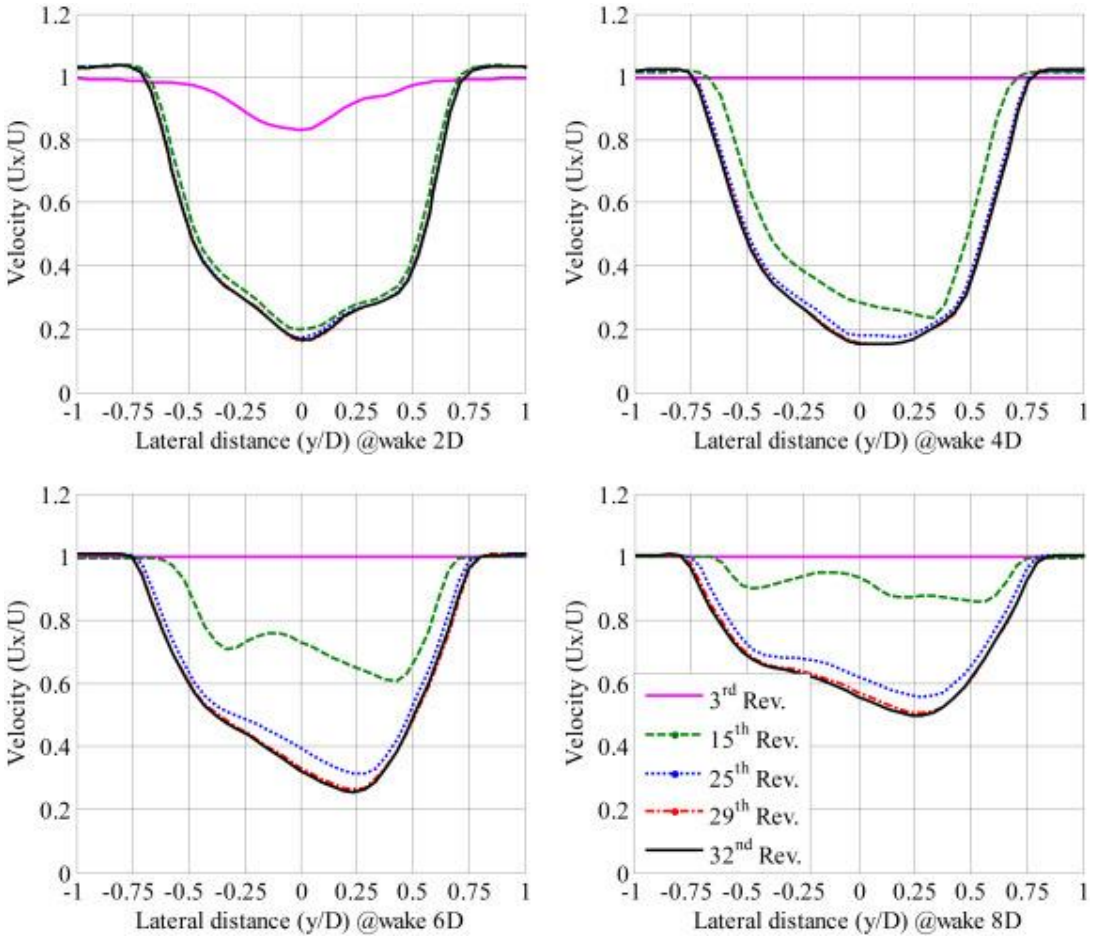

Figure 8: Stream-wise velocities from different revolutions at downstream distances [26]

J. Bremseth and K. Duraisamy [7] performed numerical analysis in 2016 to investigate the canonical problems related to VAWT arrays in order to investigate the effect of flow structure and aerodynamic interference between VAWT's. Authors found out that when VAWT's placed in a column the wake region is increased downstream due to an increase in momentum, which leads to an increase in overall power output. The author underlines that future studies concerning wind farms should reflect variable wind direction and turbulent winds. In this study flow structure and aerodynamic interference for the linear arrangement of vertical axis wind turbines has not been investigated.

S. Zanforlin and T. Nishino [27] have also performed a numerical analysis (2016) on a two-dimensional RANS simulation of VAWT to investigate the flow around a side by side VAWT and a staggered pair of VAWT. The authors examined the effect of various distances using different Tip Speed Ratio (TSR) and wind direction on the power output of two VAWT placed side by side and staggered. Results indicated that high lift and torque is produced when VAWT is placed side by side due to the change of lateral velocity approaching each wind turbine caused by the neighbouring turbine. Low power output is produced when VAWT is placed staggered. S. Zanforlin and T. Nishino [27] pointed out that the results obtained in this study is based on small land areas of wind farms and the results might vary in a larger land.

G. Mosetti, C. Poloni and B. Diviacco (1994) et.al [28] optimised the wind turbine distribution in order to produce maximum energy with minimum installation cost. A simulation-based wind farm has been produced for simplicity, with the author creating a square and sub-dividing it into 100 square cells, where each square cell presents the wind turbines location. Those wind turbines have been tested for three case studies as follows; single wind direction, the constant intensity with various wind direction and variable intensity with variable direction.

J. A. Orosa, E. J. García-Bustelo, A. C. Oliveira et.al (2009) [29] analysed the performance of a wind farm and VAWT with a wind concentrator in a typical day of the year with various climate conditions. Results indicated that wind velocity that varies with climate changes have an impact on the power generation. As a result, maximum power can be produced during the winter season and minimum power can be produced during summer. The author also mentions

that a typical wind farm performance can be maximised when a VAWT with a concentrator can be combined with HAWT where maximum power can be produced.

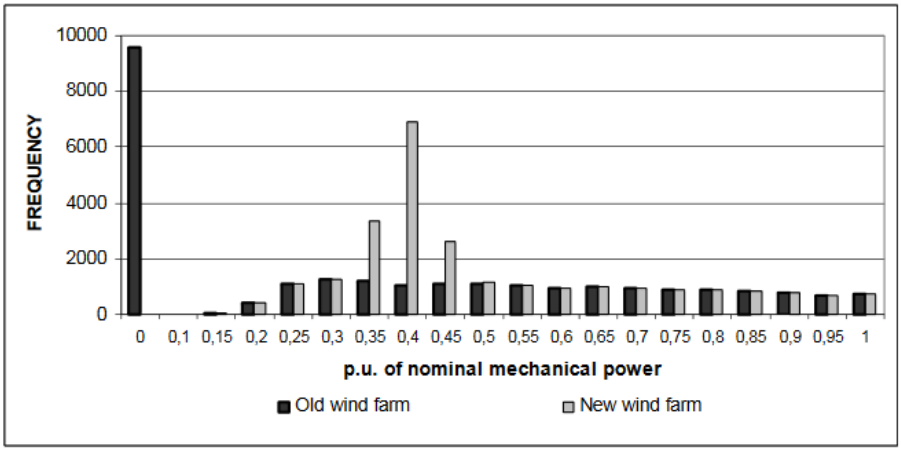

Figure 9: Old and new (with concentrator) wind farm power production under the same weather conditions [29]

Andrew Kusiak (2013) [30] has evaluated the performance of a wind farm, presented in three data curves. The power curve, blade pitch curve and rotor curve were collected using a Mahalanobis distance approach to produce a data set for modelling wind turbines. To compute the data with respect to time, Hotelling's control chart was used. The author mentions that the transformed kurtosis-skewness is a better process for monitoring condition in comparison to high-performance frequency curves.

2.3. SCOPE OF RESEARCH

The literature review presented in this chapter shows that there are insufficient detailed numerical investigations on the local flow characteristics around a single vertical axis wind turbine, although many numerical studies have performed an analysis of VAWT at various wind farm arrangements. Cautious review of the research conducted didn't present a mathematical tool that accurately specifies the distance required between VAWTS when placed in a wind farm for maximum power.

Therefore, the main aim of this study is to examine the effect of distance as a function of speed. This will initially be carried out by analysing the flow feature around a single VAWT operating in transient condition to obtain the maximum distance required to place another vertical axis wind turbine. The second aspect of this research is to compute various flow velocities to obtain the distance required in order to develop a novel prediction model for distance optimisation

that will benefit researchers and manufacturers with initial data of the distance required to place a side by side VAWT operating in any wind speed.

2.4. RESEARCH OBJECTIVES

Based on the research aim of this study and extensive literature review conducted, the following are the objectives that have been formulated:

1. To investigate the flow phenomenon around a single vertical axis wind turbine.
2. Determine the maximum distance required for positioning multiple vertical axis wind turbines without wake interference during various wind speeds.
3. Develop a mathematical tool that is used to determine the maximum distance for VAWT position in a linear arrangement.

Hence, to achieve the objectives above a 3D model has been created using Computational Fluid Dynamics tools. The next chapter will clearly present the numerical modelling techniques used in this study.

CHAPTER 3
NUMERICAL MODELLING OF VAWT

This chapter documents the design of the vertical axis wind turbine, and reviews the prototype design available in the University of Huddersfield lab. Furthermore, the use of numerical setup is discussed in detail in this chapter, aswell as the boundary condition used during this study to meet the objectives of the research. Sliding mesh technique is used to rotate the rotor blades. The scope of the work is highlighted in detail in this chapter.

3.1. PROTOTYPE DESIGN

A full-scale prototype, which is available in the mechanical labs provided by the University of Huddersfield, will be used for the experimental validation process. The prototype consists of a shaft, a rotor with 12 blades and stator with 12 blades, combined in a concentric orientation to make a wind turbine. The VAWT has an overall diameter of 2.0 m and a height of 1.0 meter. The VAWT blades have been fabricated from aluminium sheet of 1mm thickness; which has been cold rolled in order to have a fixed radius profile based on Park [31]. Aluminium has been selected as the construction material due to it being light weight, and its ability to strengthen the material after being cold rolled. The blades are arranged concentrically about the shaft axis such that they maintain an angular spacing of 30°. The stator and rotor blades are supported from the top and bottom by two support rings. The support arms are welded to a bearing housing from the centre on to the support rings; the vertical and radial position of the rotor is maintained using two taper roller bearings, which provides a fixed tip clearance of 10mm between the rotor and stator assemblies. The picture in Figure 10 below represents the prototype model.

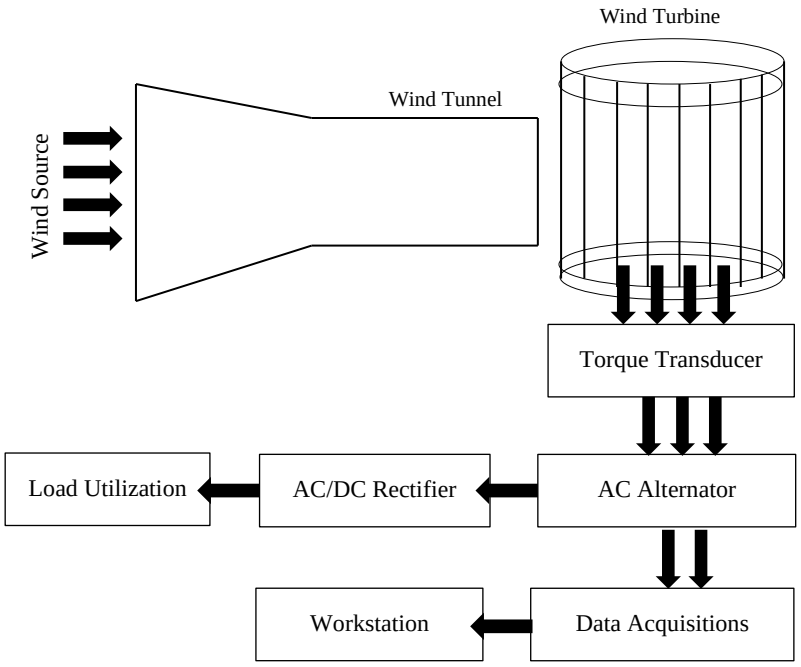

Figure 10: General Layout of the System

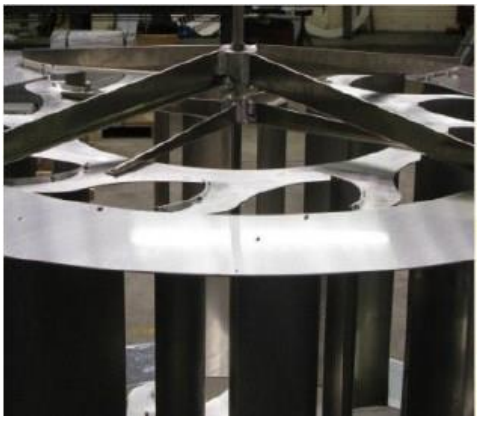


Figure 11: Prototype of the VAWT [32]

3.2. COMPUTATIONAL FLUID DYNAMICS (CFD)

Computational Fluid Dynamics is a powerful design and research tool that has been used in many industries to analyse and solve problems using numerical simulations. It complements the two approaches that are pure theory and pure experiment and provides the user with a better understanding of theory and experimental data. Since the 1960s, CFD software has been integrated into the aerospace industry to solve problems relating to research, design, development and manufacturing. In modern days, CFD is used to solve issues concerning fluid flow, heat transfer, and chemical reactions. [1]

3.3. WORKING OF CFD CODES

The three distinct streams of numerical solution techniques are the finite difference, finite element and spectral methods. The well-established CFD code is the finite volume method, a special finite difference formulation, is central to the most well-established CFD codes. The numerical algorithms are used for integrating the fundamental equations of the fluid domain. CFD codes are structured around the numerical algorithms that can tackle fluid flow problems. In order to provide easy access to their solving power, all commercial CFD packages include sophisticated user interfaces to input problem parameters and to examine the results. Hence, all codes contain three main elements [1]. These are:

- Pre-Processor
- Numerical solver
- Post Processor

Pre-Processing

Pre-processing in CFD is subdivided into two main categories, i.e. generation of the geometry model that can be created using different software such as ANSYS, SolidWorks. The geometry of the model is created using CAD modeller by means of an operator-friendly interface. The geometry created is transformed into a suitable format for the solver. At this stage, the user inputs the definition of the geometry, which is known as a computational domain. The computational domain is then divided into several small discrete elements. The process of dividing the domain is called meshing or rid generation. Meshing is an important element of the CFD process as this dictates the accuracy of the results achieved. Each element is a combination of several nodes and the combination of entire flow elements form flow domain. The meshing of the flow domain has a direct impact on the rate of convergence, processing time and solution accuracy. At the same stage, the models of the physical or chemical phenomenon are set to model the flow field. The fluid properties and appropriate boundary conditions are provided.

Numerical Solver

The numerical solver is the fundamental element of the CFD process. The solver determines fluid flow problems by using numerical methods and algorithms. The process starts with the integration of the governing equations of all control volumes in the domain. After integration, the integral forms of equations are converted into algebraic equations and finally, the solutions are calculated by iterative methods.

Post Processing

Post processing includes the examination of the results obtained and revision of the model based on these results. Results are then examined and useful data can be extracted; visualization tools can be used to extract the overall flow pattern, separation, shocks, shear layers etc. Numerical reporting tools are used to calculate quantitative results like forces, moments, average heat transfer coefficient, flux balances, surface and volume integrated quantities.

The profound use of engineering workstations has led to the development of graphic capabilities and because of this usage, CFD packages are now built with resourceful data visualisation tools. These tools are used to illustrate various features including domain geometry, grid display, vector plots, line and shaded contour plots, 2D and 3D surface plots, particle tracking, view manipulations, colour postscript output etc. Recently, animation has been added for dynamic result display. [1]

3.4. GOVERNING EQUATIONS FOR $k-\omega$ SST MODEL

The continuity, momentum, k and ω equations are solved to model the flow around the vertical axis wind turbine (VAWT). These equations are as follows:

Continuity Equation

The conservation law of mass which states that matter can neither be created nor destroyed. Using this law, the mass conservation within a control volume (CV) can be represented by the following statement. [33]

Rate of mass accumulation with a control volume	=	Rate of mass flow into a CV - Rate of mass flow out a CV

$$\frac{\partial \rho}{\partial t}+\frac{\partial}{\partial x_i}(\rho u_i)=0 \qquad \text{Equation 4}$$

Momentum Equations

$$\frac{\partial}{\partial t}(\rho u_i)+\frac{\partial}{\partial x_j}(\rho u_i u_j)=$$

$$-\frac{\partial p}{\partial x_i}+\frac{\partial}{\partial x_j}\left[\mu\left(\frac{\partial u_i}{\partial x_j}+\frac{\partial u_j}{\partial x_i}-\frac{2}{3}\delta_{ij}\frac{\partial u_l}{\partial x_l}\right)\right]+\frac{\partial}{\partial x_j}(-\rho\overline{u_i'u_j'}) \qquad \text{Equation 5}$$

Where

$-\rho\overline{u_i'u_j'}$ Reynolds stresses

Boussinesq Approach

This approach is used to relate the Reynolds stresses to the mean velocity gradients. [34]

$$-\rho\overline{u_i'u_j'}=\mu_t\left(\frac{\partial u_i}{\partial x_j}+\frac{\partial u_j}{\partial x_i}\right)-\frac{2}{3}\left(\rho k+\mu_t\frac{\partial u_i}{\partial x_i}\right)\delta_{ij} \qquad \text{Equation 6}$$

$k-\omega$ Model Equations

$$\frac{\partial}{\partial t}(\rho k)+\frac{\partial}{\partial x_i}(\rho k u_i)=\frac{\partial}{\partial x_j}\left(\Gamma_k\frac{\partial k}{\partial x_j}\right)+G_k-Y_k+S_k \qquad \text{Equation 7}$$

and

$$\frac{\partial}{\partial t}(\rho \omega)+\frac{\partial}{\partial x_i}(\rho \omega u_i)=\frac{\partial}{\partial x_j}\left(\Gamma_\omega\frac{\partial \omega}{\partial x_j}\right)+G_\omega-Y_\omega+S_\omega \qquad \text{Equation 8}$$

where

k is turbulence kinetic energy,

ω is specific dissipation rate,

G_k is the generated kinetic energy produced due to mean velocity gradients,

G_ω is the generated ω,

Γ_k and Γ_ω are the effective diffusivity of k and ω,

Y_k and Y_ω are the dissipation of k and ω due to turbulence and

S_k and S_ω are user-defined source terms

And Γ_k and Γ_ω for $k-\omega$ model are :

$$\Gamma_k = \mu + \frac{\mu t}{\sigma k} \quad \text{Equation 9}$$

$$\Gamma_\omega = \mu + \frac{\mu t}{\sigma \omega} \quad \text{Equation 10}$$

where, σk and $\sigma \omega$ are turbulent Prandtl numbers for k and ω; μt is the turbulent viscosity.

3.5. ERRORS AND UNCERTAINTY IN CFD

During the 1990s the benefits of CFD were recognised by large corporations, small and medium-sized enterprises alike, and it is now used in design/development environments across a wide range of industries. This has focussed attention on 'value for money' and the potential consequences of the wrong decision made on the basis of CFD results. The consequences of inaccurate CFD results are at best, wasted money, time and effort and at the worst, catastrophic failure of components, structures or machines. Moreover, the costs of a CFD capability may be quite substantial. [35] [33]

3.5.1. **Error**

An error is defined as a recognisable deficiency in a CFD model that is not caused by lack of knowledge. Causes of error are:

i. Numerical errors – round-off errors, iterative convergence errors and discretisation errors
ii. Coding errors – mistakes or bugs in the software
iii. User errors – human errors through incorrect use of the software

3.5.2. **Uncertainty**

It is defined as a potential deficiency in a CFD model that is caused by lack of knowledge. The main sources of uncertainty are:

1. Input Uncertainty: These inaccuracies are incorporated in the results due to non-availability or approximate representation of geometry, material properties, boundary conditions, etc.
2. Physical Model Uncertainty: These uncertainties are imparted in the solution due to inconsistencies between real flows and processes (e.g. turbulence, combustion) or due to simplifying assumptions in the modelling process (e.g. incompressible flow, steady flow) [35] [33].

3.6. GEOMETRY OF VAWT

To analyse the vertical axis wind turbine (VAWT) performance, a numerical three dimensional model of the VAWT similar to Colley [36] [15] has been created using ANSYS Fluent shown in Figure 12. The geometric details are presented in the table below:

Geometric Details of the VAWT	**Value**
Height of the VAWT (H)	1m
Outer radius of stator (Rso)	1m
Inner radius of stator (Rsi)	0.7m
Outer radius of rotor (Rro)	0.7m
Inner radius of rotor (Rri)	0.5m
Outer radius of core (Rco)	0.5m

Table 1: Geometric Details of the VAWT

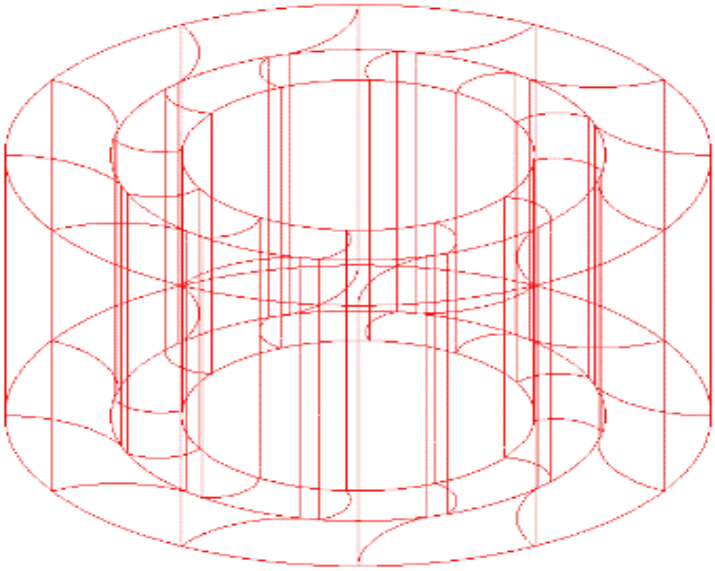

Figure 12: 3-Dimensional Model of VAWT Geometry

Figure 13 presents the dimensions of the flow domain used to simulate all the cases in this study, the length, width and height of the flow domain are 15m, 12m and 3m respectively.

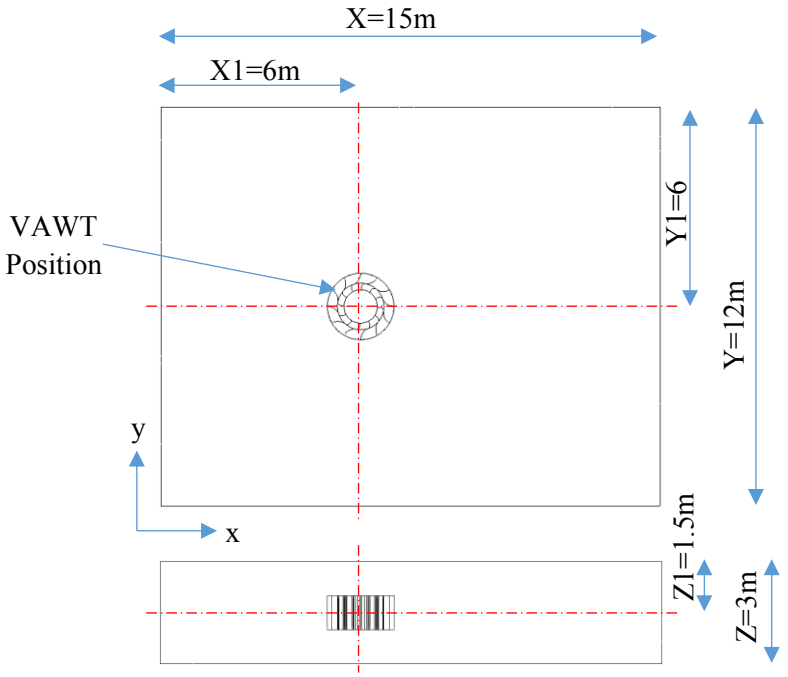

Figure 13: Domain overall Dimensions

Figure 14 presents the vertical axis wind turbine model used throughout this study; the VAWT consists of 12 stator blades and 12 rotator blades. The radius of the core region as shown is 0.5m, the radius of the rotor and stator region are 0.7m and 1m respectively. The height of the VAWT is 1 m; the geometric details of the VAWT have been obtained from the VAWT available in the mechanical lab of the University of Huddersfield.

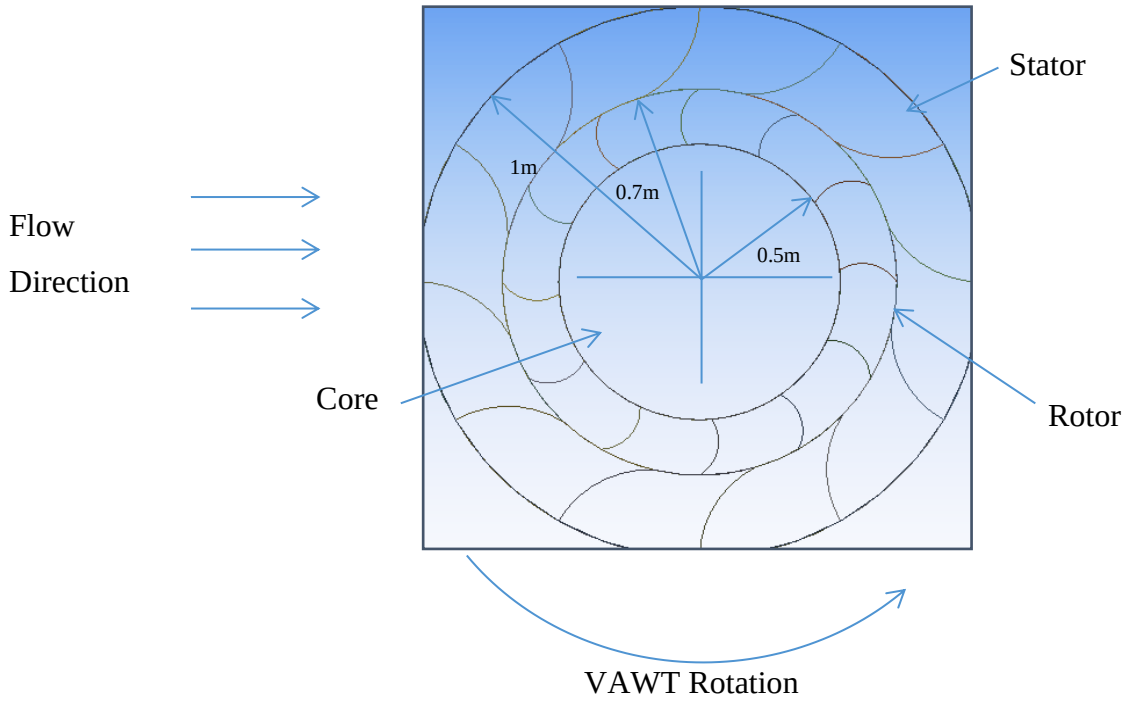

Figure 14: Vertical Axis Wind Turbine overall dimensions

3.6.1. Meshing of the Flow Domain

The mesh has been created in two steps. Global sizing has been considered in meshing the flow domain i.e. Maximum size of 135mm and minimum size of 2mm. 30mm mesh size has been chosen for stator, rotor and the core zones. The table below summarizes details of the mesh sizing used, further information of the mesh independence testing is provided in the following chapter.

Table 2: Mesh size

Zone	Maximum Size (mm)	Minimum Size (mm)
Domain	135	2
Stator	20	2
Rotor	20	2
Core	20	2

3.6.2. Mesh Type

The hybrid mesh used is a combination of tetrahedral and hexahedral mesh. Structural (hexahedral) mesh is used in the passage to obtain the same effect from every individual blade passage. Henceforth, the variable number of mesh effect from blade passage is reduced.

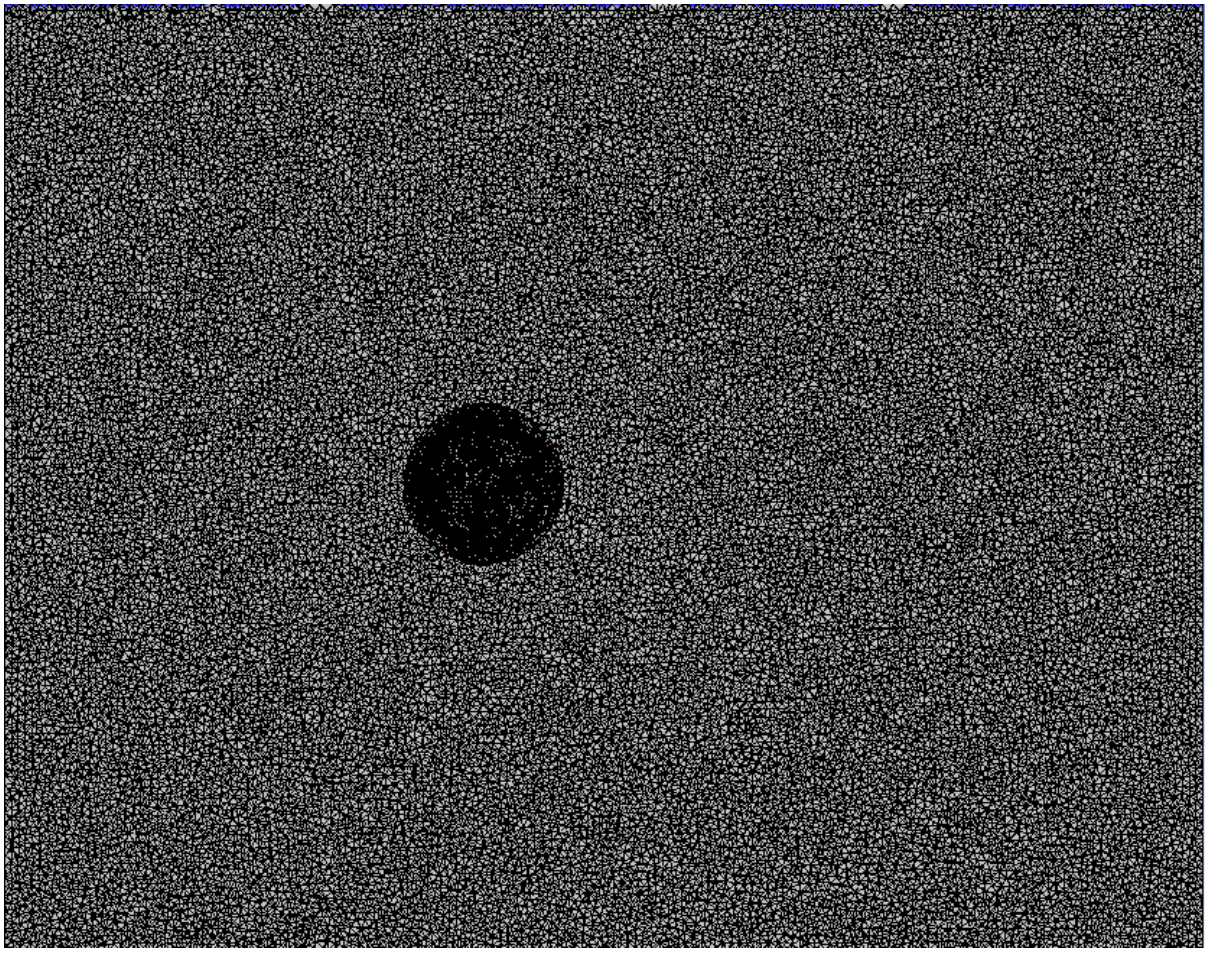

Overall Flow Domain Mesh

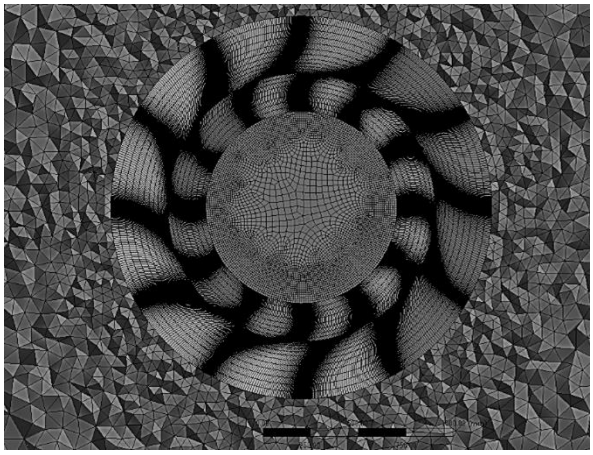

VAWT Mesh

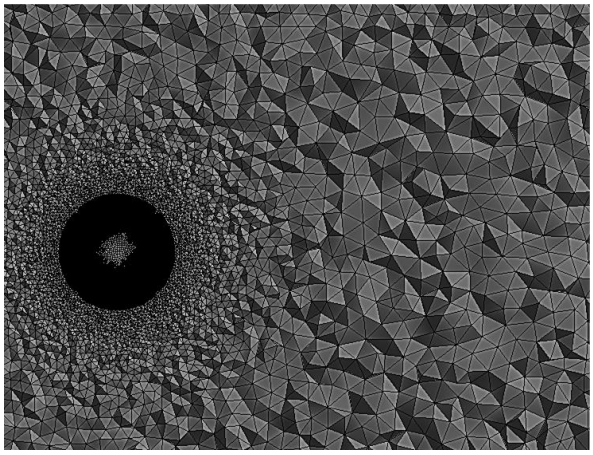

Flow Domain Mesh

Figure 15: Mesh

3.6.3. Numerical Solver

The current study is based on low-speed velocity, or annual mean wind velocity, in Huddersfield (UK) which is 4m/sec. Where the fluid is incompressible; thus pressure based solver by default is chosen. The velocity formulation of the model is set to be absolute as the fluid in the most of the domain is not rotational in nature and this ensures the smallest velocities in the frame and thereby reduces numerical diffusion in the solution leading to a more accurate solution.

Menter, F.R. [37] SST k-ω model has been used to numerically solve the flow field due to its superiority in accurately modelling the wake regions and extreme pressure regions that is caused at the leading edge of the airfoil. SST k-ω model has a proven reliability for achieving numerical accuracy for lower pressure gradients. Where it consists of two additional transport equations that represent turbulent properties of the flow. SST ensures that the model equations behave appropriately in both near-wall region and far-field zones using the blending function. This blending function is designed to be operating one of the near wall region (k-ω model) and zero away from the wall surface (transformed k-ε model). It contains equations for turbulent viscosity which has a major effect on the performance of VAWT. The model also calculates the exact dissipation rate for the transport of the mean-square vorticity fluctuation rather than using the constant in the calculation. This model provides more accurate results and captures fluid flows with rotation, separation and re-circulation which are the key parameters for the VAWT performance.

In order to achieve accuracy in the results, pressure-velocity coupling, gradient and spatial discretisation settings have been incorporated in the simulation. The Navier-Stokes equations used in the model are solved in a discretised form which refers to linear dependence of the velocity on the pressure as well as of the pressure on the velocity. To predict the pressure distribution in the flow domain, pressure – velocity coupling has been employed for this purpose. Also, a SIMPLE algorithm is used for faster and reliable results and the approximation of the velocity is acquired by solving momentum equation. The pressure gradient is calculated from the pressure distribution which is calculated from the previous iteration using a pressure-velocity coupling. This helps in calculating new pressure distribution and velocities based on the solution of previous pressure distribution. The velocities are used to calculate a new set of conservative fluxes. In order to construct the values of a scaler at the cell faces for computing secondary diffusion terms and velocity derivatives, gradients are required.

Green-Gauss node-based gradient evaluation has been employed to calculate the values at a node from the surrounding cell–centered values on arbitrary unstructured meshes by solving a constrained minimization problem, preserving a second-order spatial accuracy.

The discrete values of the scalars are stored at the cell centres. However, for the convection terms, the face values are calculated by interpolating the results from the cell centres and this is achieved by using an upwind spatial discretisation scheme. In the upwinding method, the face value is calculated from quantities in the cell upstream or upwind relative to the direction of the normal velocity. Second order upwind schemes are being utilised in this study to acquire pressure, momentum, turbulent kinetic energy and turbulent dissipation rate and for its accuracy of results.

3.6.4. Boundary Conditions

The flow in the domain is defined by the boundary conditions. Hence, conditions for inlet, outlet, walls, and object in flow are defined at this stage. Also, the fluid properties are identified at this stage. The fluid used in the simulations is air and its properties have been incorporated in the study. The tables below demonstrate the boundary conditions that have been used for the simulation model. Five different inlet velocities have been chosen for this study, being 4m/s, 8m/s, 12m/s, 16m/s and 20m/s respectively. 0.5 TSR (λ) has been chosen during the five cases of this study. Colley [37], the outlet boundary is set at a zero-gauge pressure in order to impart actual atmospheric conditions. The top, front and bottom walls in the flow domain have been set at as free slip boundaries and the rear wall has been set up as a no-slip condition. The no-slip boundary condition represents the zero-velocity gradient between the walls and the flow layer adjacent to the wall. The interactions between the stator blades and rotor blades have been modelled using sliding mesh technique because of its transient nature.

Table 3: Boundary Conditions of Case Study 1

Boundary Name	**Boundary Type**	**Boundary Condition**
Inlet	Velocity Inlet	4m/sec
Outlet	Pressure Outlet	Atmospheric Conditions
Rotor Blades	Rotating Walls	No-Slip
Stator Blades	Stationary Walls	No-Slip

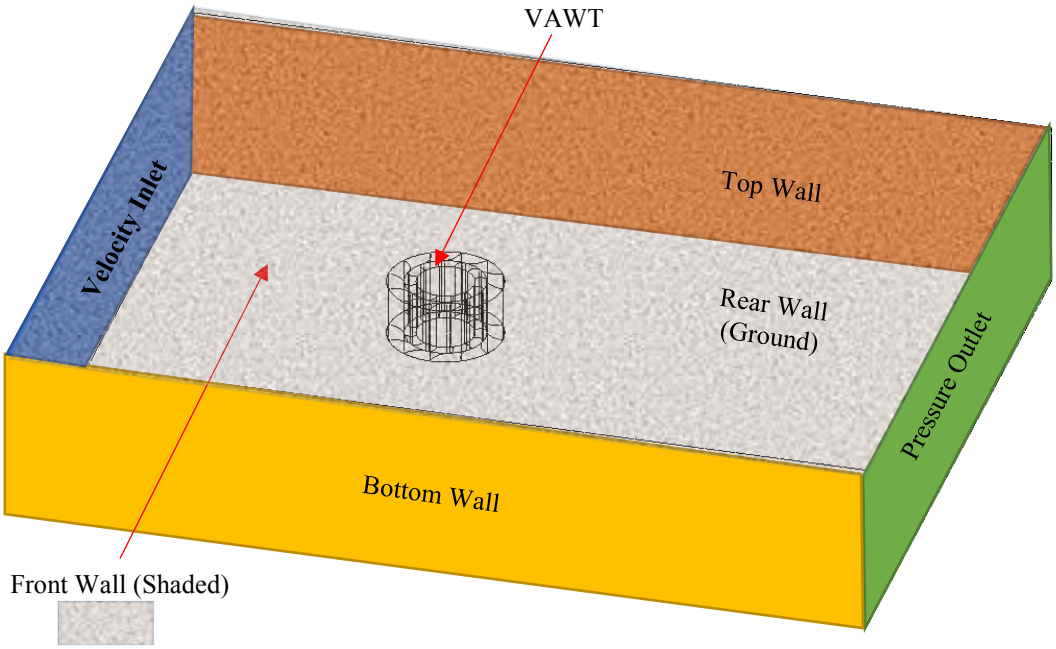

Figure 16: 3D View Showing Boundaries of Flow Domain

Table 4: Boundary Conditions of Case Study 2

Boundary Name	Boundary Type	Boundary Condition
Inlet	Velocity Inlet	8m/sec
Outlet	Pressure Outlet	Atmospheric Conditions
Rotor Blades	Rotating Walls	No-Slip
Stator Blades	Stationary Walls	No-Slip

Table 5: Boundary Conditions of Case Study 3

Boundary Name	Boundary Type	Boundary Condition
Inlet	Velocity Inlet	12m/sec
Outlet	Pressure Outlet	Atmospheric Conditions
Rotor Blades	Rotating Walls	No-Slip
Stator Blades	Stationary Walls	No-Slip

Table 6: Boundary Conditions of Case Study 4

Boundary Name	Boundary Type	Boundary Condition
Inlet	Velocity Inlet	16m/sec
Outlet	Pressure Outlet	Atmospheric Conditions
Rotor Blades	Rotating Walls	No-Slip
Stator Blades	Stationary Walls	No-Slip

Table 7: Boundary Conditions of Case Study5

Boundary Name	Boundary Type	Boundary Condition
Inlet	Velocity Inlet	20m/sec
Outlet	Pressure Outlet	Atmospheric Conditions
Rotor Blades	Rotating Walls	No-Slip
Stator Blades	Stationary Walls	No-Slip

3.6.5. Sliding Mesh

Sliding mesh is a novel meshing method utilized in rotating bodies such as rotor-stator in a vertical axis wind turbine, where the time-accurate solution is used. In this technique, multiple reference frames (cell zones) are connected to at least one interface zone to the opposite cell zone. The mesh interface is formed by connecting the interface zones of adjacent cell zones. Throughout the calculation, the cell zone will move relative to each other and will slide (rotate) in discrete steps. Figure 17 represenst the multiple cell zones in this research study, as the rotation takes place between the rotor and the stator node alignment of the mesh faces is not required on the mesh interface since the flow in this study is unsteady.

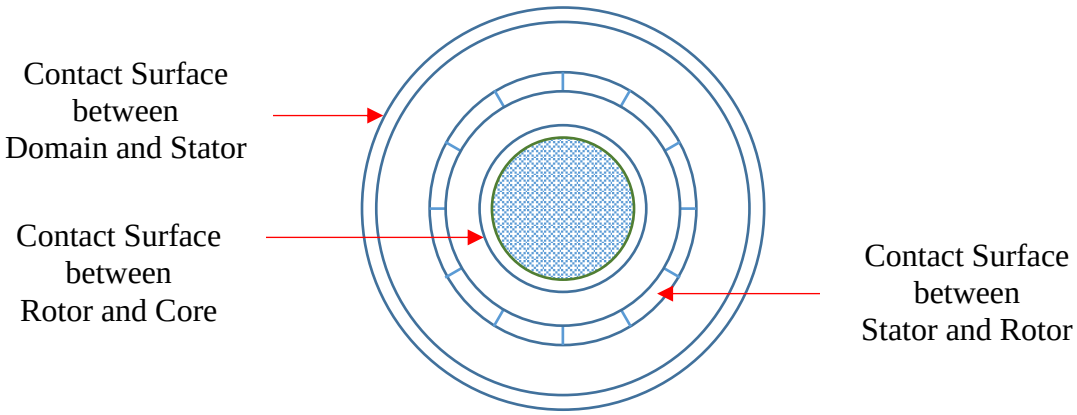

Figure 17: Interface zones

Conservation equation formulation for the dynamic mesh is employed to characterise the sliding mesh. This is because the mesh motion in the sliding mesh formulation is rigid (all cells retain their original shape and volume). The integral form of the conservation equation with a moving boundary for a general scalar ($\emptyset$) on an arbitrary control volume (V) is denoted as

$$\frac{d}{dt}\int_V \rho\emptyset dV + \int_{\partial V} \rho\emptyset\left(\vec{u} - \overrightarrow{u_g}\right).d\vec{A} = \int_{\partial V} \Gamma\nabla\emptyset\,.d\vec{A} + \int_V S_\emptyset dV$$

Where ρ = Fluid Density,

$\vec{u}$ = Flow Velocity Vector,

$\overrightarrow{u_g}$ = Mesh Velocity of the Moving Mesh,

Γ = Diffusion Coefficient,

$S_\emptyset$ = Source Term of $\emptyset$ and

∂V = Boundary of the Control Volume (V)

The time derivative in the equation above can be represented as

$$\frac{d}{dt}\int_V \rho\emptyset dV = \frac{(\rho\emptyset V)^{n+1} - (\rho\emptyset V)^n}{\Delta t}$$

Where n and $n+1$ denote the respective quantity at the current and next time level. Where V^{n+1} is computed from

$$V^{n+1} = V^n + \frac{dV}{dt}\Delta t$$

Where, $\frac{dV}{dt}$ is the volume time derivative of the control volume; the time rate of change of the cell volume is zero therefore the equation simplifies to

$$V^{n+1} = V^n$$

Hence to satisfy the mesh conservation law; the control volume is computed from

$$\sum_j^{n_f} \vec{u}\, g.j.\vec{A}\, j = 0$$

Where n_f is the number of faces on the control volume and $\vec{A}\, j$ is the j face area vector. The dot product $\vec{u}g.j.\vec{A}\, j$ on each control volume face is calculated from

$\vec{u}\, g.j.\vec{A}\, j = \frac{\delta V_j}{\Delta t}$ where δV_j is the volume swept out by the control volume face j over the time step Δt.

Sliding mesh method has been used in this study in order to rotate the rotor blades. This technique captures the transient flow phenomena occurring during rotor/stator blade interaction and hence provides more realistic results.

3.6.6. Convergence Criteria

It is vital to get a converged solution that specifies that the solution has reached a steady state and the variations in the flow parameters, w.r.t. the iterative process of the solver, have expired. Consequently, only a converged solution can be treated as one which predicts the solution of the flow problem with reasonable accuracy.

The convergence criteria set for the continuity, velocities in three dimensions and the turbulence parameters in ANSYS 17.2 is 0.00001. This means that when the change in the continuity, velocities and turbulence parameters drops down to the fourth place after the decimal, the solution is treated as a converged solution. However, in many practical applications, the default criterion does not necessarily indicate that the changes in the solution parameters have died out. Hence, it is often better to monitor the convergence rather than relying on the default convergence criteria.

In the present study, the vertical axis wind turbine rotor blades have been monitored throughout the iterative process. The solution has been considered converged once it has become statistically steady i.e. the variations in the torque output become negligibly small between three consecutive rotations of the VAWT. After numerically simulating the flow of air in the vicinity of VAWT, various results have been composed of CFD. Detailed discussions on these results are presented in the following chapters.

3.7. SCOPE OF THE WORK

Outline of Mesh Independence

Initially, a mesh independence testing study is carried out to analyse the results obtained from three configurations of mesh elements which approximately form 1 million, 2 million and 4 million mesh elements. Figure 18 presents the outline of the study.

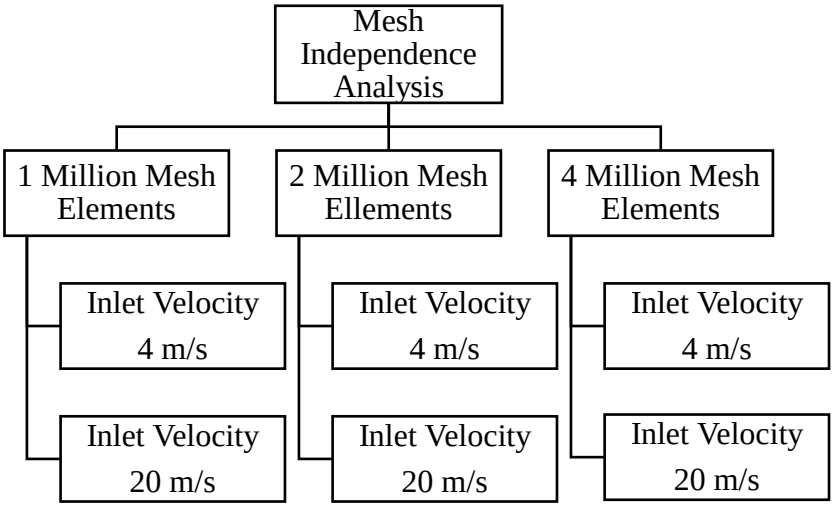

Figure 18: Outline of Boundary Conditions for Mesh Independence Study

Outline of the Time-Step Independence

Subsequently, a time-step based analysis is carried out to ascertain the accuracy of the results obtained from various time-step configurations for establishing the accuracy of the results. Figure 19 presents the outline of the study.

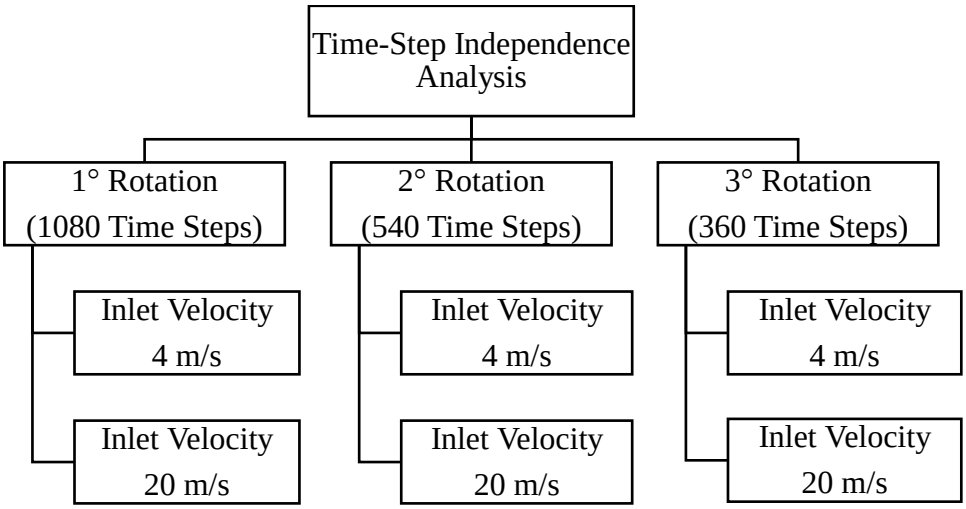

Figure 19: Outline of Boundary Conditions for Time-Step Independence Study

Outline of the Simulation Studies for Optimization

Finally, the results obtained from the mesh independence and time step studies are analysed. The analysis showed that the mesh size configuration for 4 million elements and 3° angular rotation time steps are of significant accuracy as presented in section 4.2 and 4.3, respectively. Based on these studies, the simulation studies for obtaining the optimum inter-distance between VAWTS are conducted.

Figure 20 outlines the five different studies are performed under various inlet velocities.

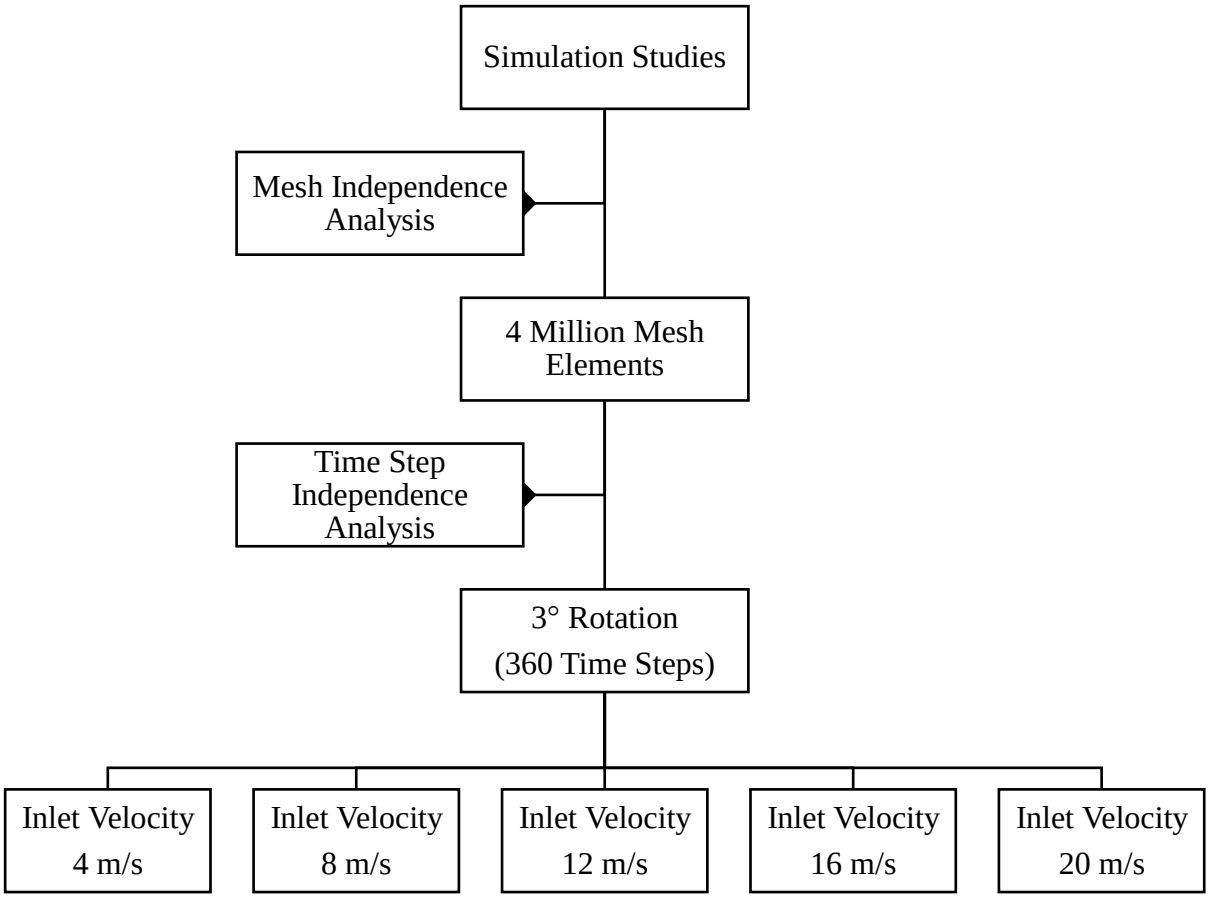

Figure 20: Outline of Boundary Conditions for Simulation Studies

Chapter 4
Numerical Results

The primary focuses of this chapter are mesh sensitivity testing, along with time step independence testing in order to accurately analyse the performance of the VAWT. Further analysis has been carried out in this chapter to underline the questions highlighted in the current literature. Therefore, a flow field analysis was carried out to accurately determine the optimal distance under five different wind velocities. After conducting a numerical analysis on the VAWT a novel mathematical tool that is used for distance optimisation between VAWT's was established.

4.1. VERTICAL AXIS WIND TURBINE PERFORMANCE

Sliding mesh method has been utilized as a part of this research in order to clearly investigate the transient behaviour of the flow around the vertical axis wind turbine. In this method, rotor blades change their position with respect to the stator blades. Consequently, the geometrical design of the VAWT consistently differs. As a result, performance analysis of the VAWT that consists of 12 stator blades and 12 rotor blades placed at an angle of 30º with respect to each other operating under transient condition has been analysed through this study.

In order to analyse the performance of the vertical axis wind turbine, the flow at various blade angle position is analysed. It can be seen in Figure 21 that high-pressure is generated at the windward of the VAWT due to the blade orientation. It can be clearly seen as the VAWT rotates the pressure at the leeward of the VAWT is increased when comparing Figure 21 and Figure 22. Therefore, it can be concluded that the VAWT depicts high-pressure region at the windward due to the obstruction effect, thus the flow enters the VAWT through the flow passages that is further explained using the velocity variation contours.

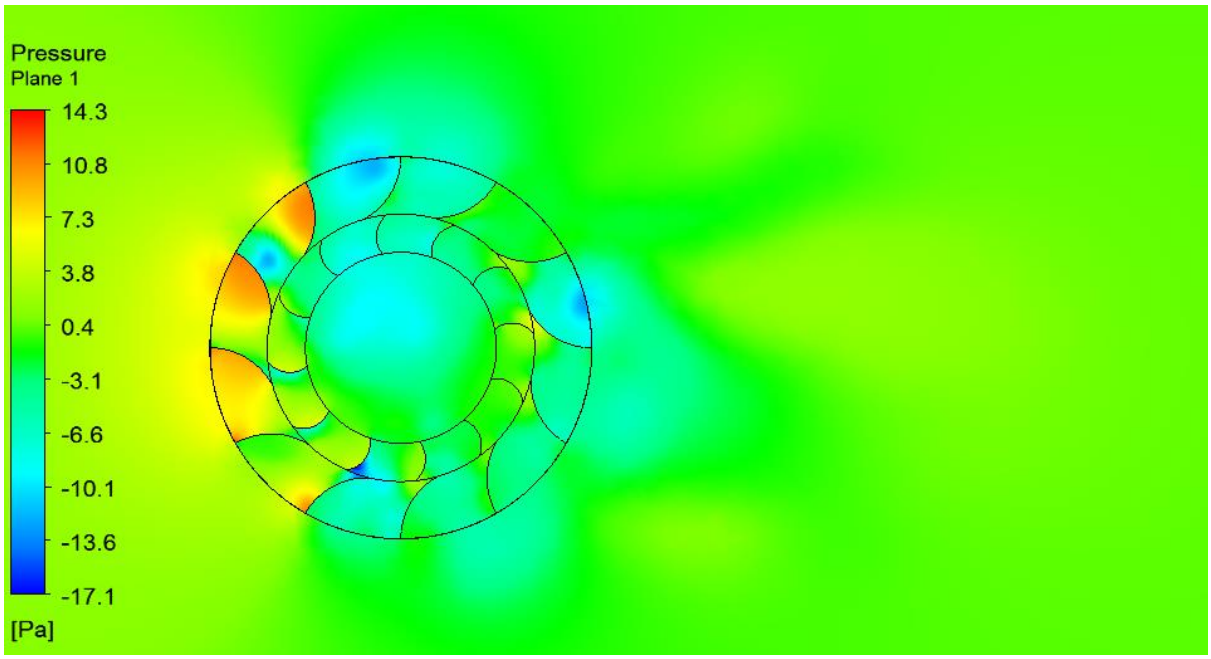

Figure 21: Pressure Variation at 4m/s after 45° of Rotation

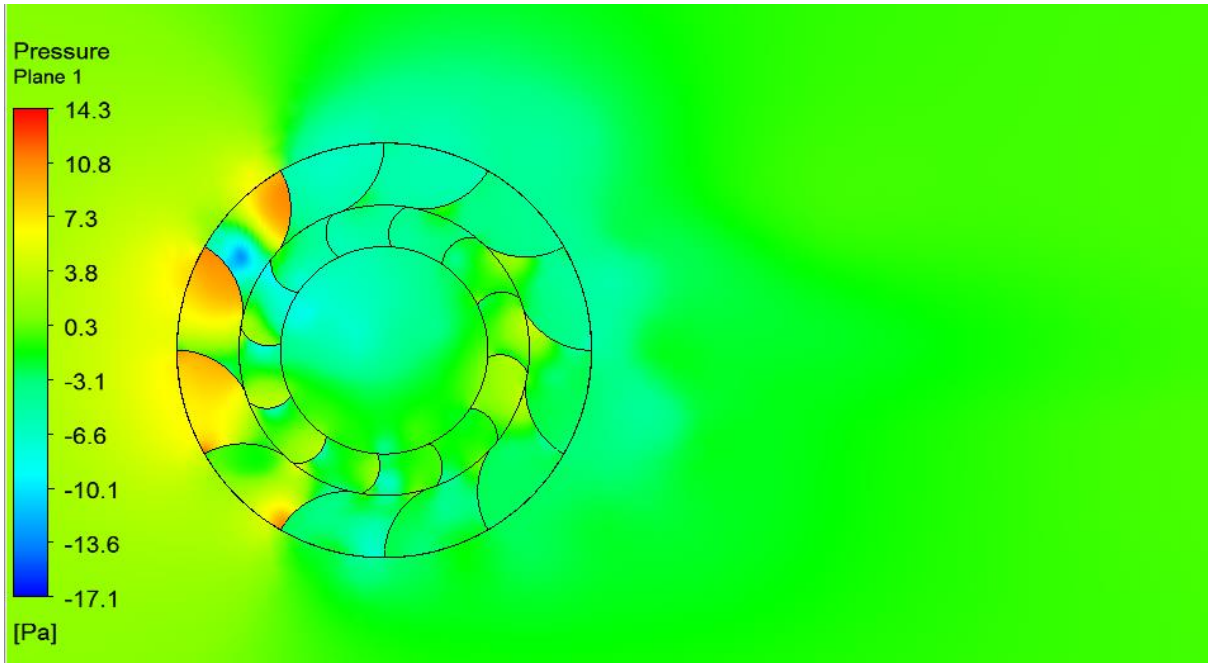

Figure 22: Pressure Variation at 4m/s after 360° of Rotation

It can be clearly identified from Figure 23 and Figure 24 that the flow velocity is highly affected by the blade orientation, which thereby forms flow velocity passages at the windward. It can be identified that the free stream velocity (4m/s) increases up to (6.4m/s) considering this specific study. Therefore, it can be concluded that the performance of the VAWT depends on the angular position of the blade.

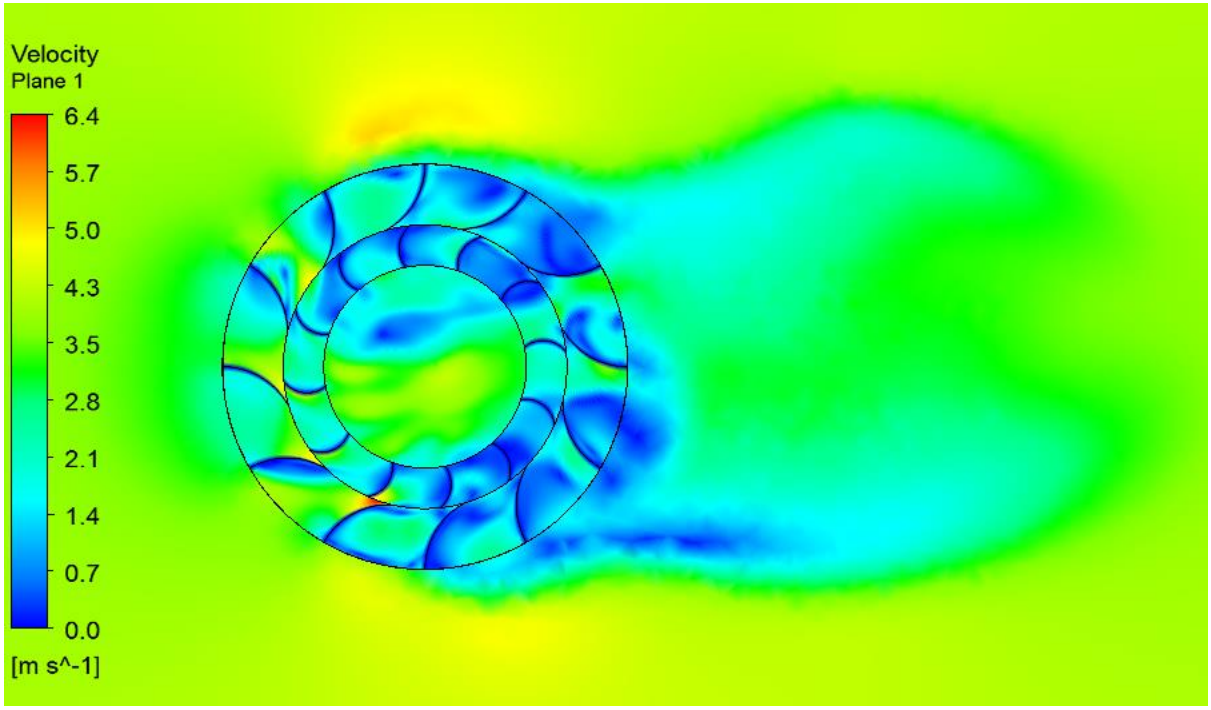

Figure 23: Velocity Variation at 4m/s after 45° of Rotation

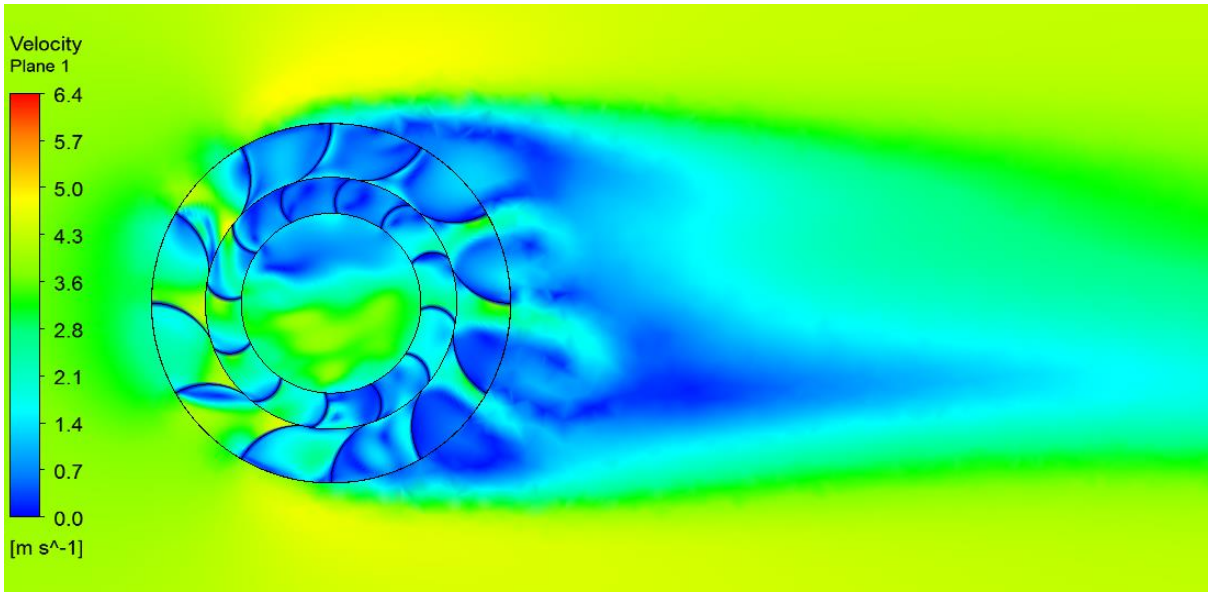

Figure 24: Velocity Variation at 4m/s after 360° of Rotation

From Figure 25 it can be seen that the numerical simulations conducted in this research are based on the performance of the VAWT, wherein the results obtained during the third revolution are considered (720-1080) angle degrees. Initially, at the first revolution, negative torque is produced due to CFD software that attempts to spin the turbine. At this stage, the turbine does not produce torque, but consumes it. The flow around the VAWT starts to develop gradually in the first and second revolution and upon reaching the third revolution, the flow pattern is significantly consistent where the turbine starts to produce torque. The variation in the torque coefficient from initial start-up to 3rd revolution is shown in Figure 25.

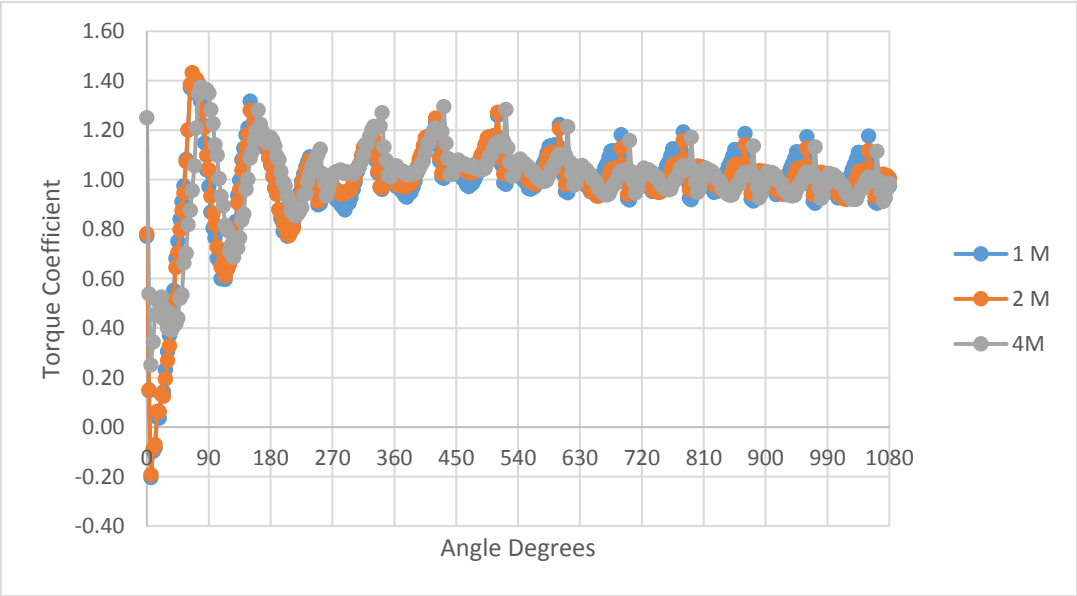

Figure 25: Instantaneous Torque Coefficient (1st to 3rd Revolution) for 4m/s

In order to capture the flow phenomenon accurately, the results obtained from the 3rd revolution are considered throughout all studies. The torque coefficients associated with the VAWT for the 3rd revolution are shown in Figure 26.

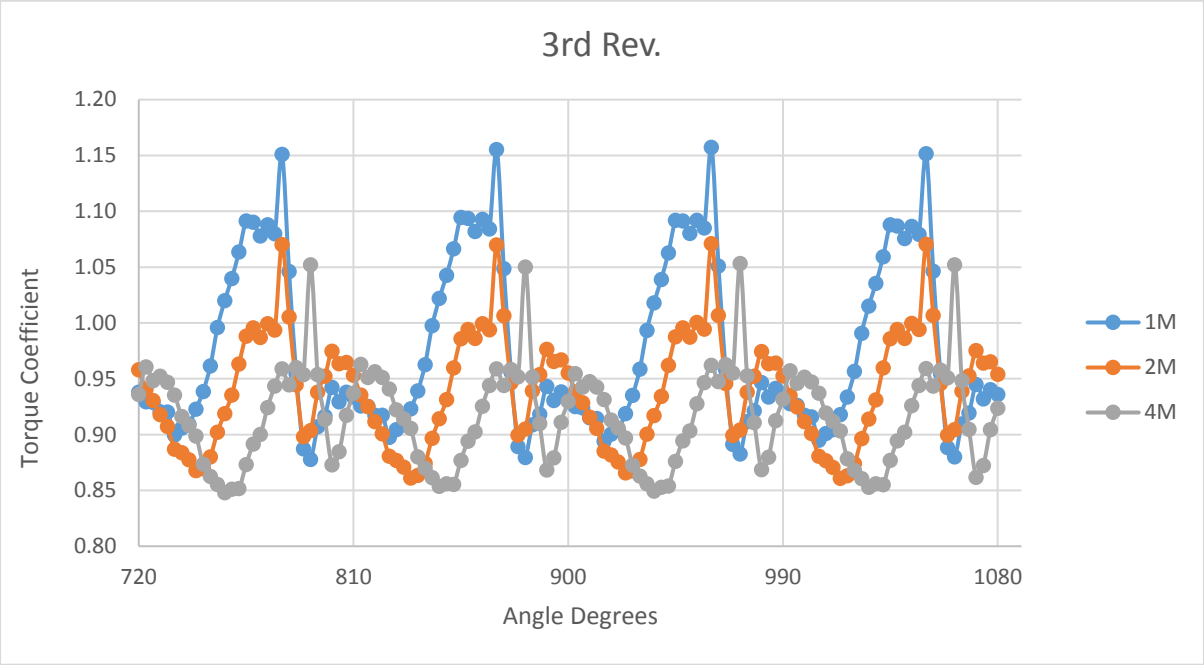

Figure 26: Instantaneous Torque Coefficient (3rd Revolution Only) for inlet velocity 4m/s

The torque output of a vertical axis wind turbine can be calculated using equation:

$$T = \frac{1}{2} C_T \rho v^2 A R$$

where

T = Torque Generated (Nm)

C_T = Torque Coefficient

ρ = Fluid Density (Air = 1.225kg/m^3)

v = Average Freestream Wind Velocity (m/s)

A = Projected Area of the VAWT (m^2)

R = Radius of Rotor Blades (m, R = 0.7)

Torque Coefficient, C_T thus can be calculated as follows:

$$C_T = \frac{2T}{\rho v^2 A R}$$

In order to efficiently analyse the performance of the vertical axis wind turbine (VAWT), the following flow and performance parameters have been critically analysed in the present study:

1. Axial flow velocity in the vicinity of the VAWT will be analysed
2. Iso-surface in the vicinity of the VAWT
3. The deficit of the velocity at a different location in the vicinity.

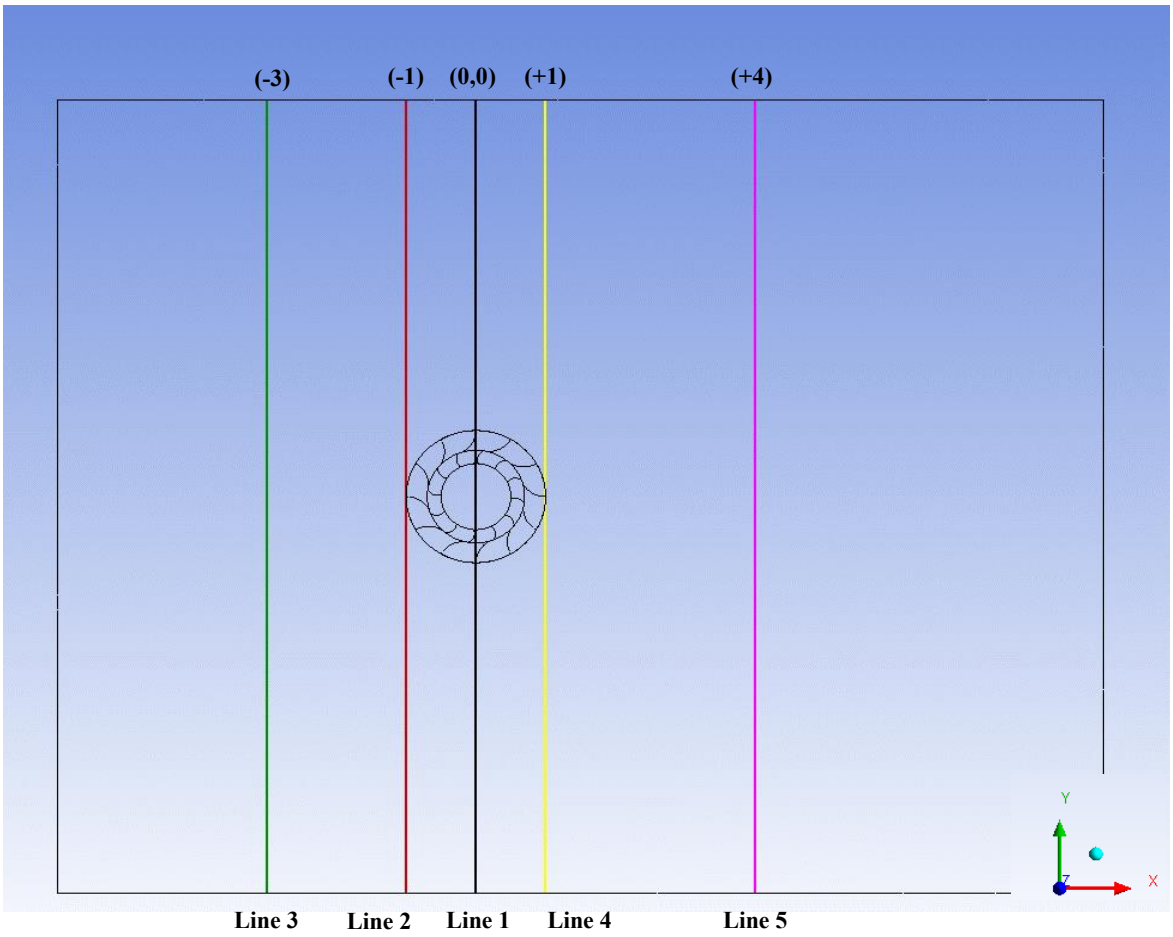

Figure 27: Lines Position for Axial Velocity in x-direction

Figure 27 presents the (x-y) location of the velocity (u) lines in the vicinity. Line 3 presents the axial velocity 3m away from the VAWT upstream, line 2 is axial velocity at the entrance of the VAWT, line 1 is the axial velocity at the centre of the VAWT, line 4 is the axial velocity at the exit of the VAWT, and line 5 is the axial velocity 4m away from the VAWT downstream. The lines will be further plotted for the five studies to visualise the flow velocity at this specific location in order to clearly understand the flow phenomena and velocity deficit in each study.

4.2. MESH INDEPENDENCE TESTING

In this research, three different meshes with 1, 2 and 4 million mesh elements were chosen for mesh independence testing. Mesh sensitivity has been utilised to obtain accurate time-bound results. Two mesh independence studies for each of the 4m/s and 20m/s flow velocities were performed with 1 million, 2 million and 4 million mesh elements. The average torque obtained from these studies is provided in Table 8. For an inlet velocity of 4 m/s with 4 million mesh elements, the average torque variation from 2 million mesh elements is found to be -2.37%, whereas the difference between 2 million and 1 million mesh elements is 4%.

No. of elements (million)	Mesh		Velocity (m/sec)	λ	ω (rad/sec)	Torque (Nm)	Percentage Difference (%)
	Min	Max					
1035063	2 mm	175 mm	4	0.5	2.86	6.68	-
2056310	2 mm	135 mm	4	0.5	2.86	6.42	-4.00
4070293	2 mm	105 mm	4	0.5	2.86	6.27	-2.37

Table 8: Mesh Independence Testing for 4m/s

The results obtained from the mesh analysis of 20m/s inlet velocity is shown in Table 9. It follows the same trend as that of the 4m/s and depicts a variation of 2.28% from 2 million elements to 4 million elements.

No. of elements (million)	Mesh		Velocity (m/sec)	λ	ω (rad/sec)	Torque (Nm)	Percentage Difference (%)
	Min	Max					
1035063	2 mm	175 mm	20	0.5	14.29	168.41	-
2056310	2 mm	135 mm	20	0.5	14.29	154.36	-9.10
4070293	2 mm	105 mm	20	0.5	14.29	157.97	2.28

Table 9: Mesh Independence Testing for 20m/s

From these studies, it can be concluded that the results obtained from 4 million mesh elements is capable of predicting accurate results and hence, all the studies in further simulations are based on 4 million mesh elements.

4.3. TIME STEP INDEPENDENCE TESTING

Three different time step sizes for each of the two velocities, 4m/s and 20m/s are used to ascertain the optimal time-step size. The results for both 4m/s and 20m/s velocities are shown in Table 10 and Table 11.

Time step size	Average Torque (Nm)	Average Power (Watts)	Percentage Difference (%)
1deg	6.27	17.92	-
2deg	6.02	17.19	-4.21
3deg	5.89	16.82	-2.24

Table 10: Time Step Independence Testing for 4m/s

Time step size	Average Torque (Nm)	Average Power (Watts)	Percentage Difference (%)
1deg	157.97	2256.67	-
2deg	151.48	2163.96	-4.28
3deg	148.11	2115.88	-2.27

Table 11: Time Step Independence Testing for 20m/s

From Table 10, it is depicted that the variation in the average torque from 2 degrees to 3 degrees is 2.24%, whereas from 1 to 2 degrees is 4.21%. Also, a similar trend is depicted in Table 11 for 20m/s inlet flow velocity. To acquire accurate results and less simulation time, 3-degrees time step size is thus used in all studies.

Figure 28 and Figure 29 shows the instantaneous torque results captured from ansys for the third revolution only. Figure 28 shows the results for time step independence for free stream velocity 4m/s and Figure 29 shows the results for time step independence for free stream velocity 20m/s. As seen that the percentage difference between 3 degrees 4m/s and 3 degrees 20m/s is less than 0.2 %, and so a 3-degree time step will be used for all other free stream velocities considered in this study such as 8m/s, 12m/s, 16m/s and 20m/s.

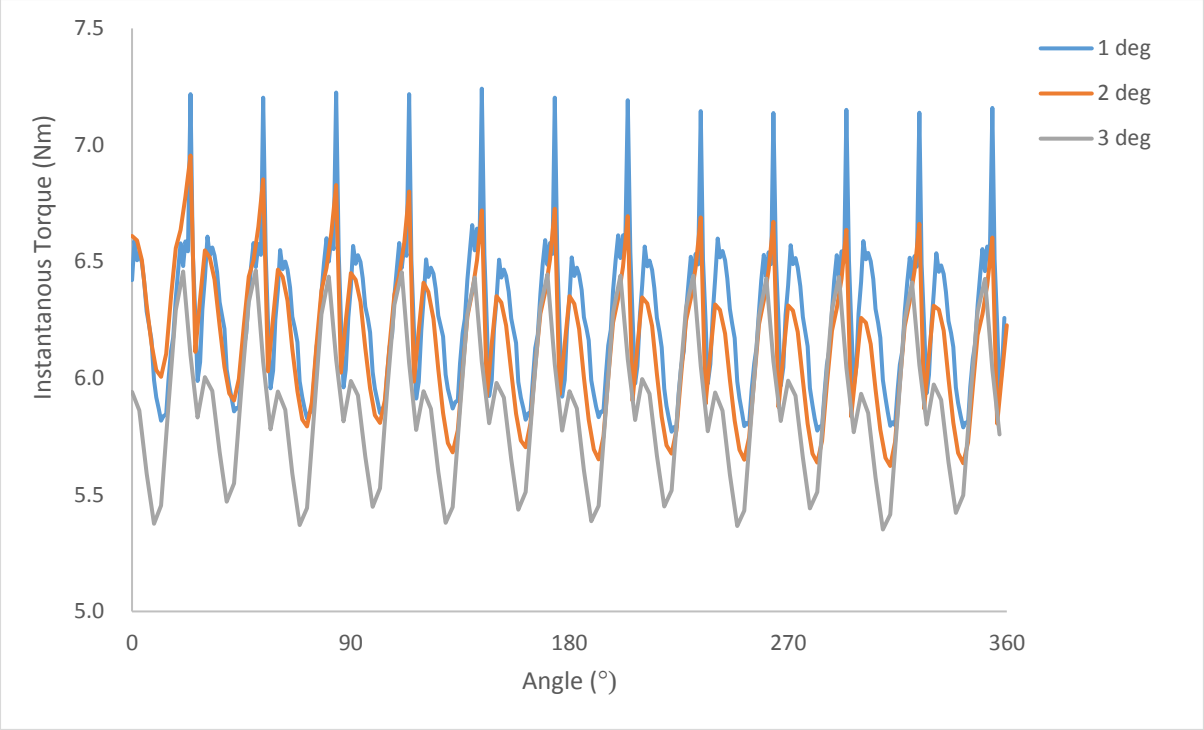

Figure 28 Time Step Independence Testing 4m/s

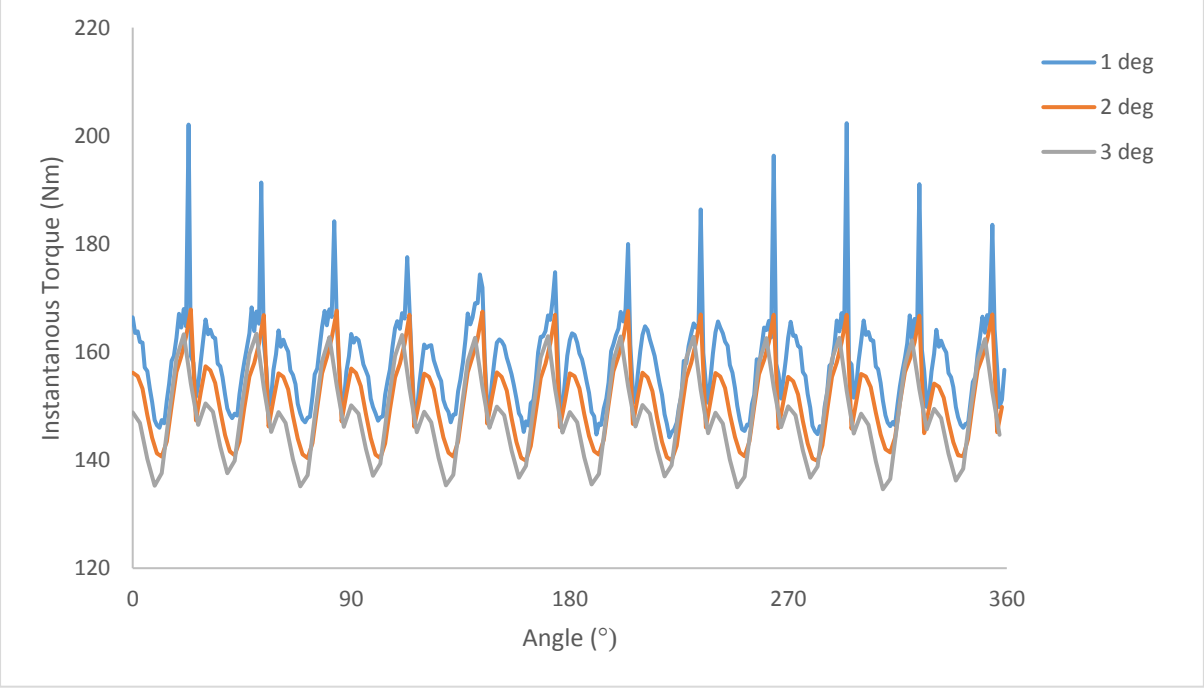

Figure 29 Time Step Independence Testing 20m/s

4.4. FLOW FIELD ANALYSIS

The following analysis investigates the velocity field in the radial direction (velocity u) so that the flow distribution can be analysed. This velocity field is presented using an iso-surface tool from CFD post to clearly demonstrate the wake region. The velocity field that is presented in the study cases is in the form of V/Vavg where Vavg is taken from the free stream area weighted average at the velocity inlet boundary. There are five studies that have carried out in this research to clearly investigate the flow field around a single VAWT operating under a wind velocity of 4m/s, 8m/s, 12m/s, 16m/s and 20m/s respectively.

The aim of this section is to establish the region where the flow field is affected by the turbine, where 5% more than the inlet velocity is used to establish the minimum distance between two turbines, and 5% less than the inlet velocity is used to ensure that the inlet is remote from the pressure zone.

Case Study 1 (4m/s)

Figure 30 depicts the x-y projected area of the wake at 5% more than the inlet free stream velocity. Due to the wide formation of the wake at the leeward of the vertical axis wind turbine, it can be seen that the maximum distance is then probed to identify the maximum surface that the wake can occupy when operating under velocity 4m/s. It can also be seen that the wake region at the right of the VAWT is higher, this is due to the axis of rotation.

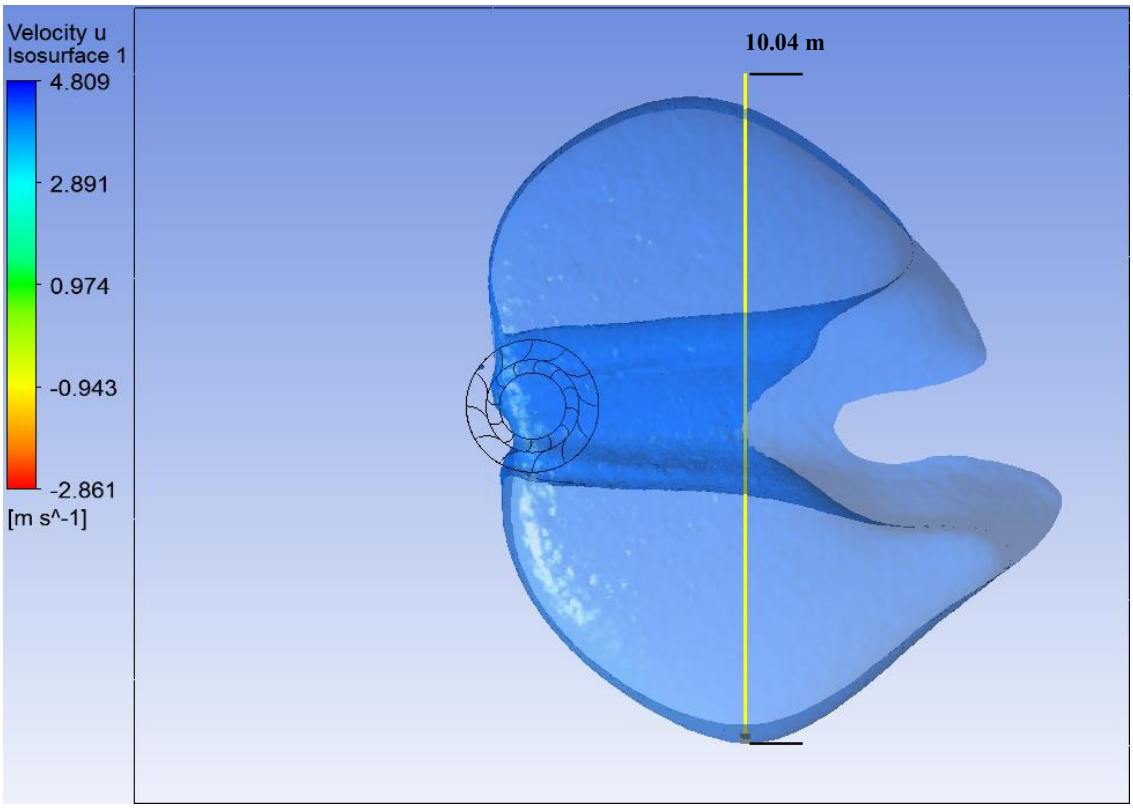

Figure 30: Spatial distribution of velocity set at 5% more than the inlet velocity (4m/s)

Figure 30 depicts the wake region formed at 5% more than the inlet velocity 4m/s in order to establish the minimum distance between two turbines shown to be 10.04m. Any turbine placed inside the wake region will be affected by the turbine and will not operate under normal flow conditions.

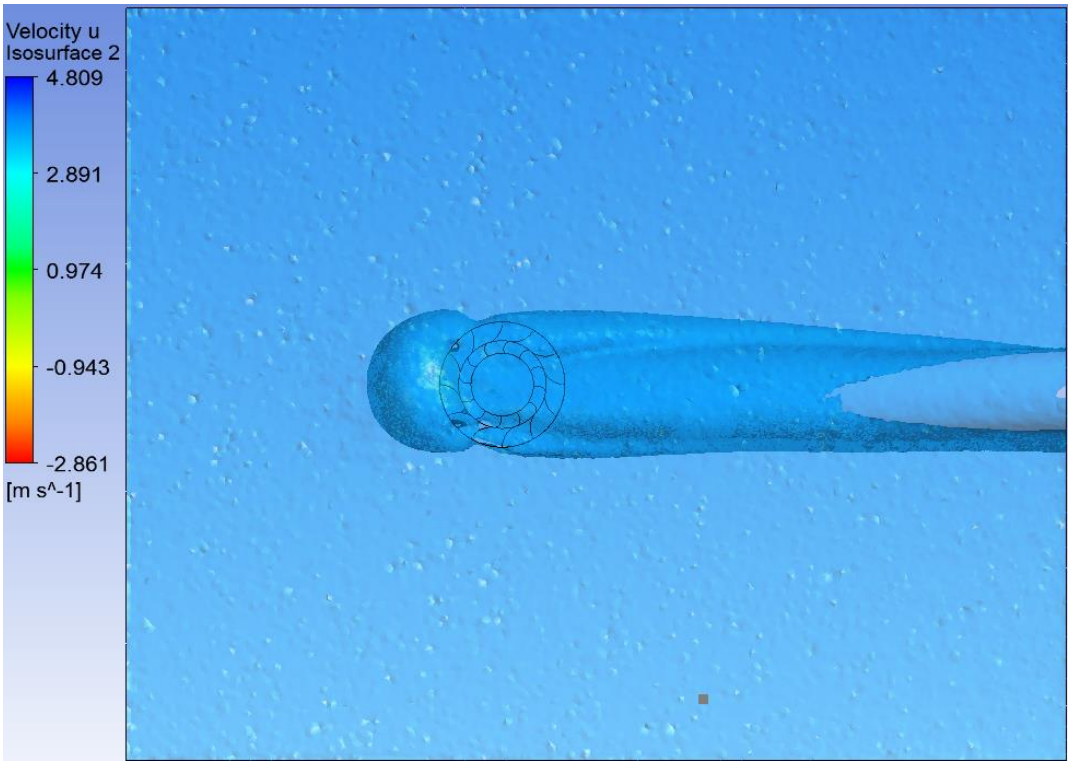

(a) Top view

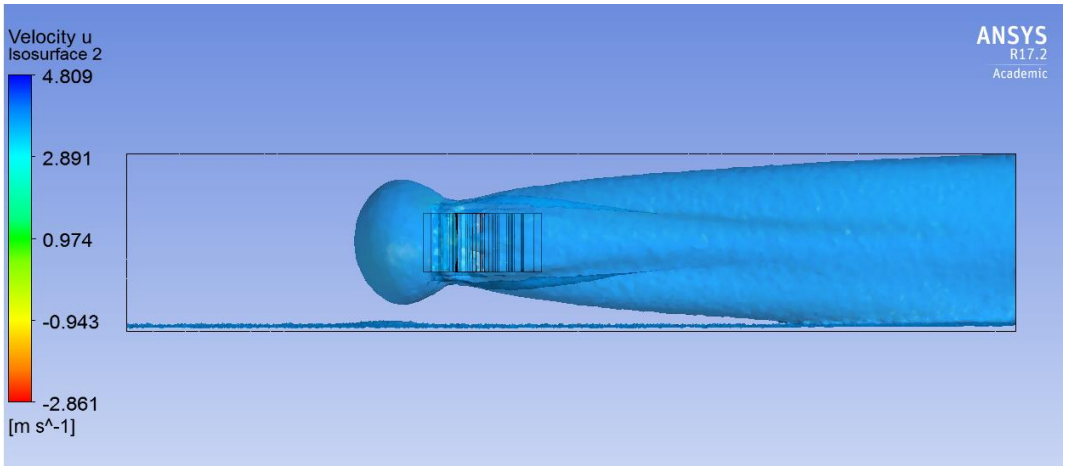

(b) Side view

Figure 31: Spatial distribution of velocity set at 5% less than the inlet velocity (4m/s)

Figure 31 (a) depicts the top view of the wake region 5% less than the inlet velocity and Figure 31 (b) depicts the side view of 5% less than the inlet velocity 4m/s. From Figure 31 it can be clearly seen that the inlet is far-off from the pressure zone surrounding the VAWT. It can also be seen that the inlet velocity speed 4m/s is decreased around the VAWT region due to the

VAWT that acts like an obstruction. The velocity at the leeward of the VAWT is highly affected and a wake is formed as shown in Figure 31 (a) (b).

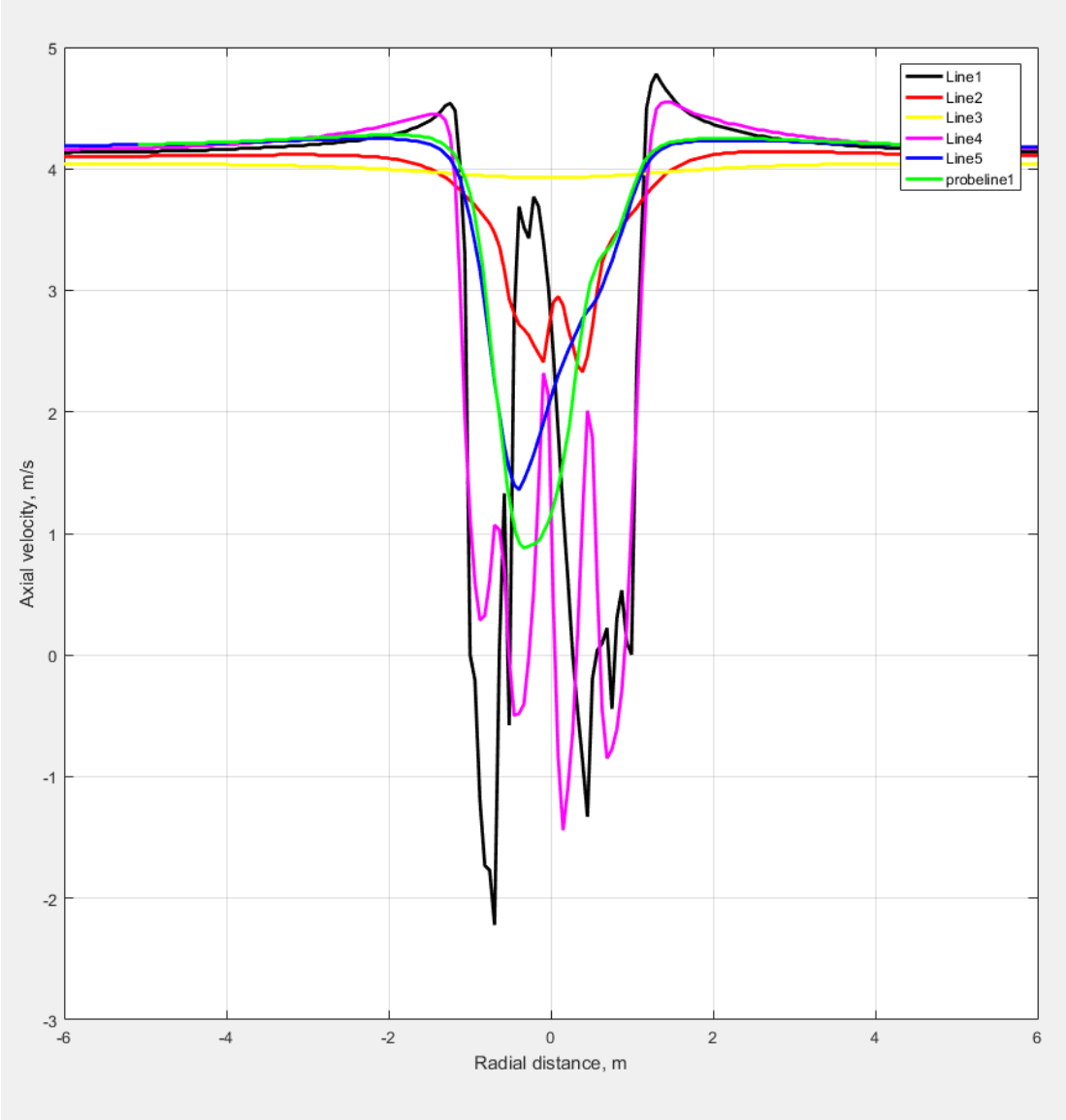

Figure 32: Axial velocity 4m/s as a function of Radial Distance

Figure 32 depicts the axial velocity deficit as a function of radial distance for 4m/s. Line 3 shows that the upstream velocity is not affected, inlet flow velocity 4m/s remains constant. Line 2 presents the axial velocity at the windward of the turbine and the two peak and valleys signify that the air is entering the VAWT. Line 1 depicts the flow phenomena at the centre of the VAWT. Line 4 depicts the flow exiting the turbine where it carries the highest peaks and valleys; this signifies that the fluid is exiting the VAWT from the various stator and rotor blades. Line 5 describes the flow at the leeward 4m away from the turbine; one valley signifies

that the flow is recovering and will gain its actual velocity. It can be seen that the strongest deficits were found at the leeward of the turbine due to shear and high turbulence generation.

Case Study 2 (8m/s)

Similar to Case Study 1 (4m/s) Figure 33 shows the x-y projected area of the flow in u direction. It shows the wake region at 5% more than the inlet free stream velocity (8m/s). Using Iso-surface tool from post-process, the maximum distance can be probed to be 4.9m. As Case Study 1, it can be clearly seen that the wake region at the right of the VAWT forms longer wake effect, this should be taken in consideration when measuring the maximum distance in the Y direction. It can be concluded that the maximum distance required to place another VAWT is 9.7m.

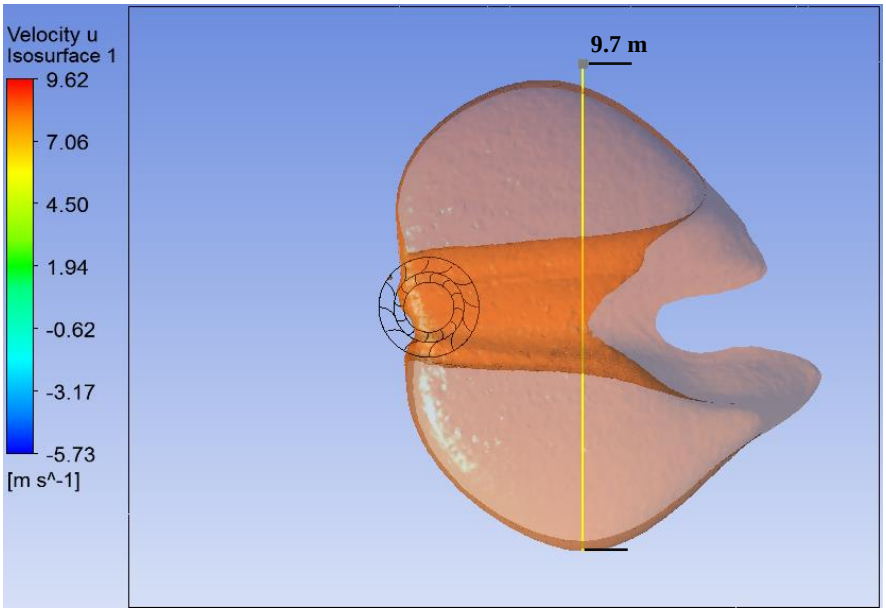

Figure 33: Spatial distribution of velocity set at 5% more than the inlet velocity (8m/s)

It can be clearly seen that the maximum distance measured in Figure 33 at 5% more than the inlet free stream velocity 8m/s is less than the maximum distance measured in Figure 30 5% more than the inlet velocity 4m/s. The maximum distance measured at Figure 33 is 9.7m any turbine placed inside the wake region will be affected by the neighbouring turbine and will not operate under normal wind conditions.

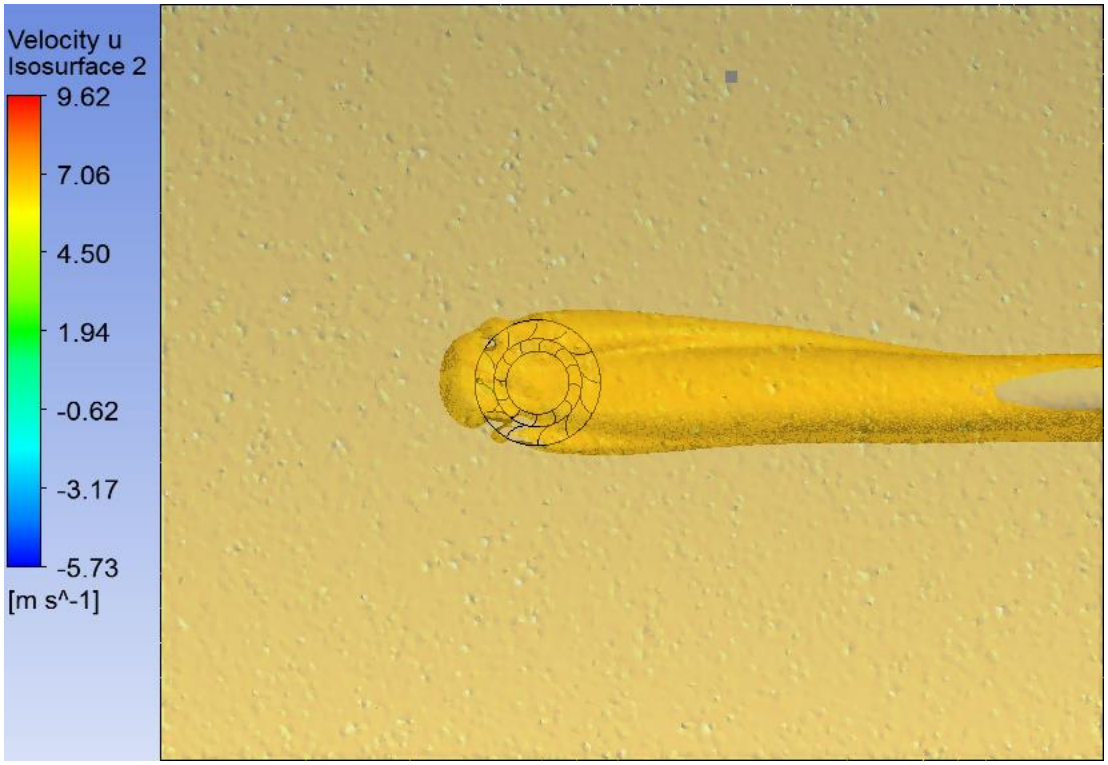

(a) Top view

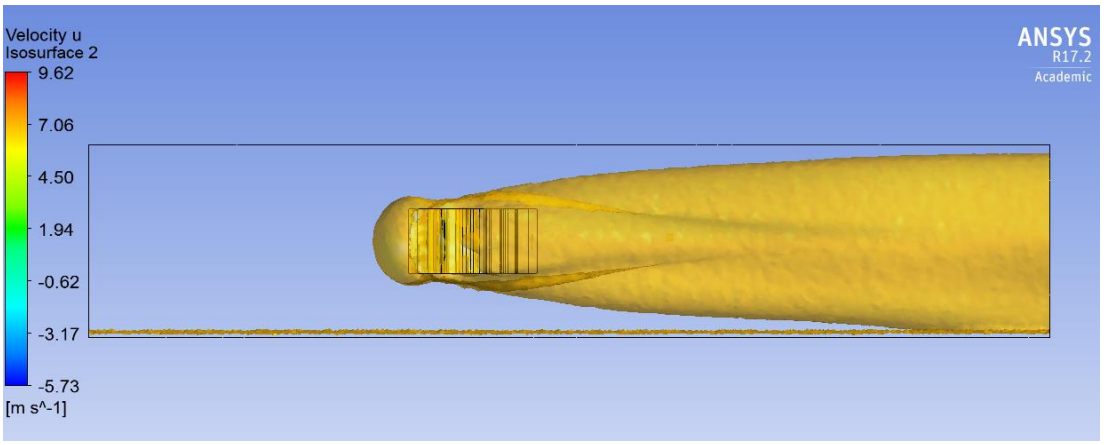

(b) Side view

Figure 34: Spatial distribution of velocity set at 5% less than the inlet velocity (8m/s)

Figure 34 (a) depicts a top view of the wake region 5% less than the inlet velocity (8m/s) and Figure 34 (b) depicts the side view of 5% less than the inlet velocity 8m/s. It represents the flow formation in z-x cross section. From this figure, it can be clearly seen that the inlet is distant from the pressure zone surrounding the VAWT. It can also be seen that the free stream velocity 8m/s is decreased around the VAWT region due to the VAWT that acts like an obstruction. As in Figure 31 when the operating free stream velocity was 5% less than 4m/s; the velocity at the leeward of the VAWT is highly affected and a wake is formed as shown in

Figure 34 (a) (b). The wake form the same shape in Figure 31, Figure 34 although the operating speeds differ.

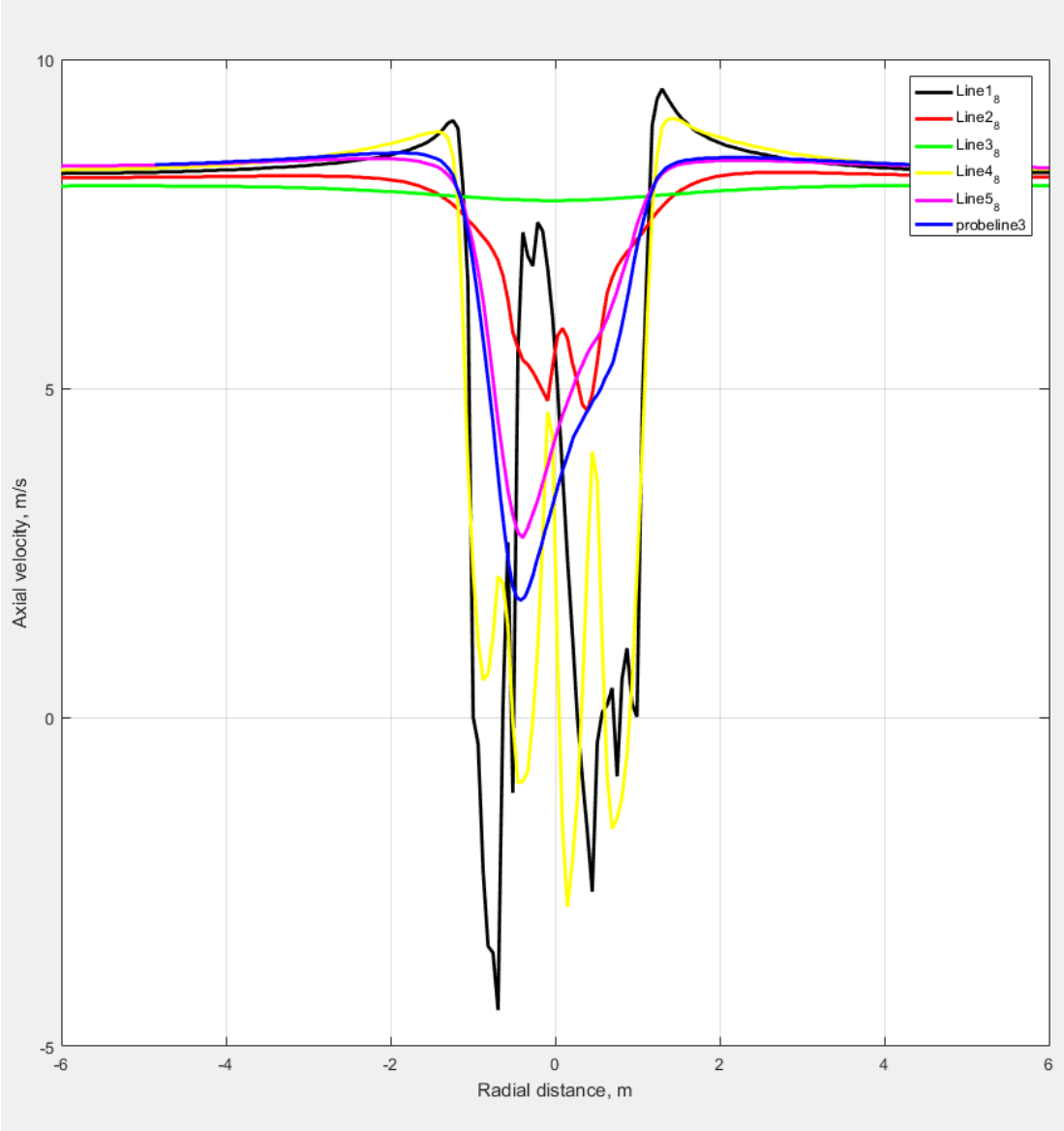

Figure 35: Axial velocity 8m/s as a function of Radial Distance

Figure 35 depicts the axial velocity as a function of radial distance for 8m/s. Line 3 shows that the upstream velocity 8m/s is not affected and the flow velocity remains constant. Line 2 presents the axial velocity at the windward of the turbine and the two peak and valleys signify that the air is entering the VAWT. Line 1 depicts the flow phenomena at the centre of the VAWT; this line shows the steepest peak and valleys due to circulations of the fluid particles. Line 4 depicts the flow exiting the turbine where it carries the highest peaks and valleys. Line 5 describes the flow at the leeward 4m away from the turbine. It can be seen that the strongest deficits were found at the leeward of the turbine due to shear and high turbulence generation.

Case Study 3 (12m/s)

Similar to Case Study 1 and Case Study 2, Figure 36 represents an x-y projected area of the wake in u direction. It depicts the wake region at 5% more than the inlet free stream velocity (12m/s). Using Iso-surface tool from post-process, the maximum distance can be probed to be 4.8m. As in Case Study 1 and 2, it can be clearly seen that the wake region at the right of the VAWT forms longer wake effect and this should be taken in consideration when measuring the maximum distance in the Y direction. It can be concluded that the maximum distance required to place another VAWT is 9.6m.

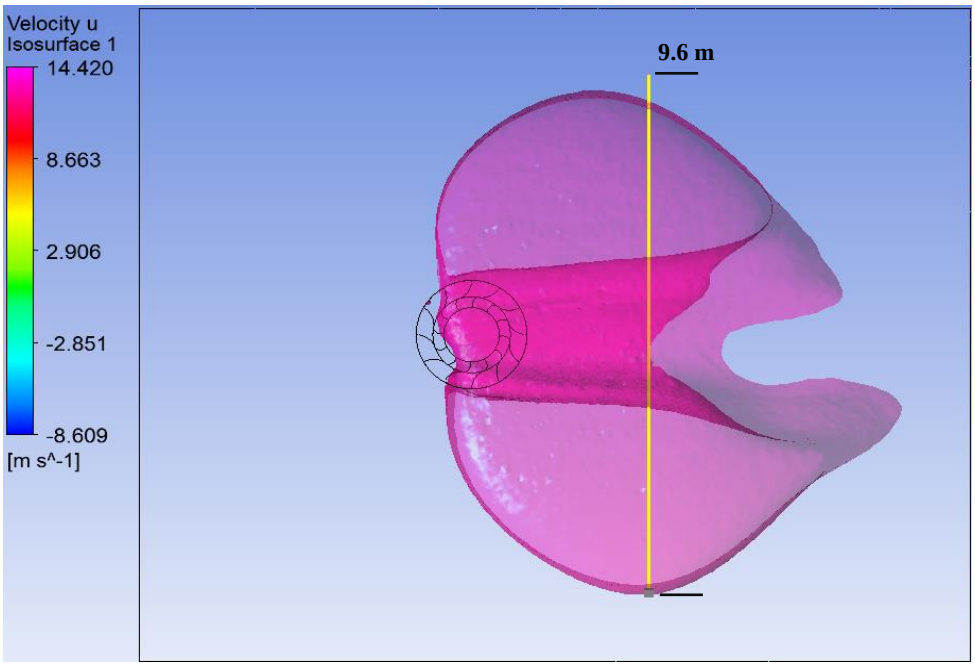

Figure 36: Spatial distribution of velocity set at 5% more than the inlet velocity (12m/s)

Comparing Figure 36 to Figure 30 and Figure 33 it can be clearly identified that the maximum distance probed is decreased when measured at 5% more than the inlet velocity. The maximum distance measured at Figure 36 for 5% more than the inlet velocity 12m/s is 9.6m any turbine placed inside the wake region will be affected by the neighbouring turbine and will not operate under normal wind conditions.

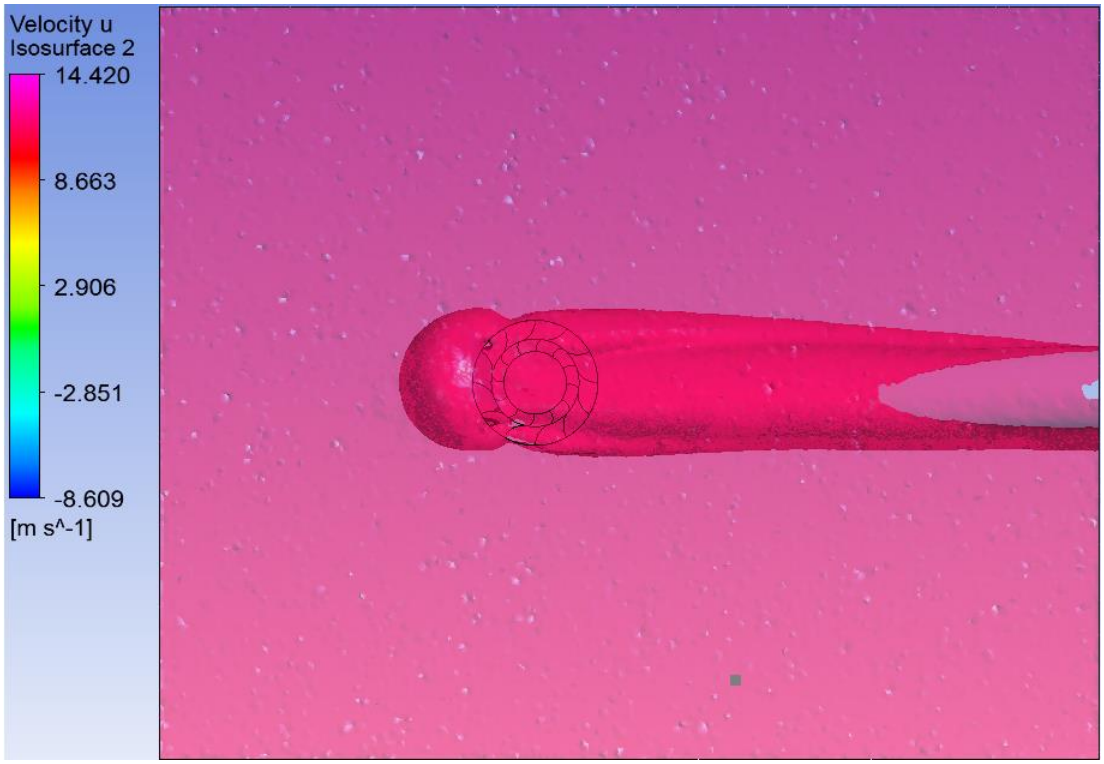

(a) Top view

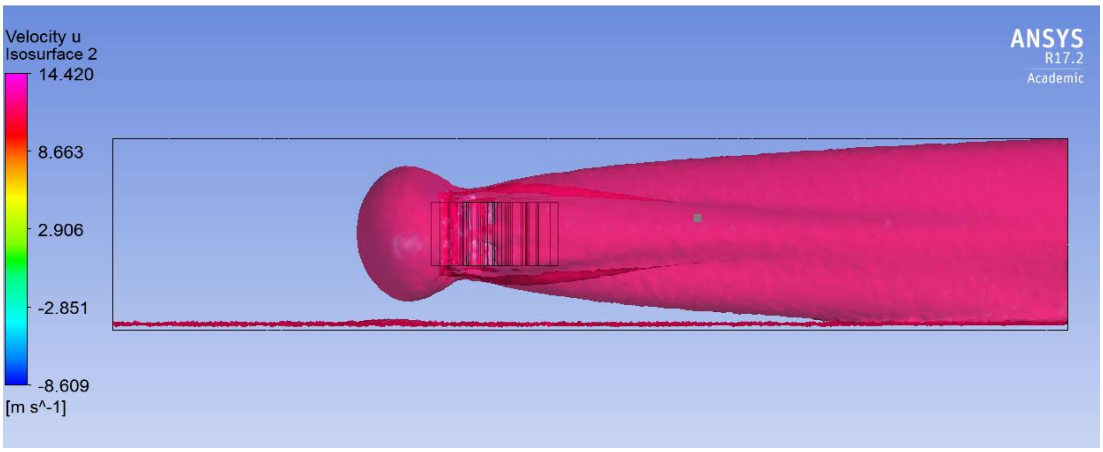

(a) Side view

Figure 37: Spatial distribution of velocity set at 5% less than the inlet velocity (12m/s)

Figure 37(a) depicts a top view of the wake region 5% less than the inlet velocity (12m/s) and Figure 37(b) depicts the side view of 5% less than the inlet velocity 12m/s. It represents the flow formation in z-x cross section. From this figure, it can be clearly seen that the inlet is distant from the pressure zone surrounding the VAWT. It can also be seen that the free stream velocity 12m/s is decreased around the VAWT region due to the VAWT that acts like an obstruction. As in Figure 31 and Figure 34; the velocity at the leeward of the VAWT is highly

affected and a wake is formed as shown in Figure 37(a) (b). The wake forms the same shape as in Figure 31 and Figure 34 although the operating speeds differ.

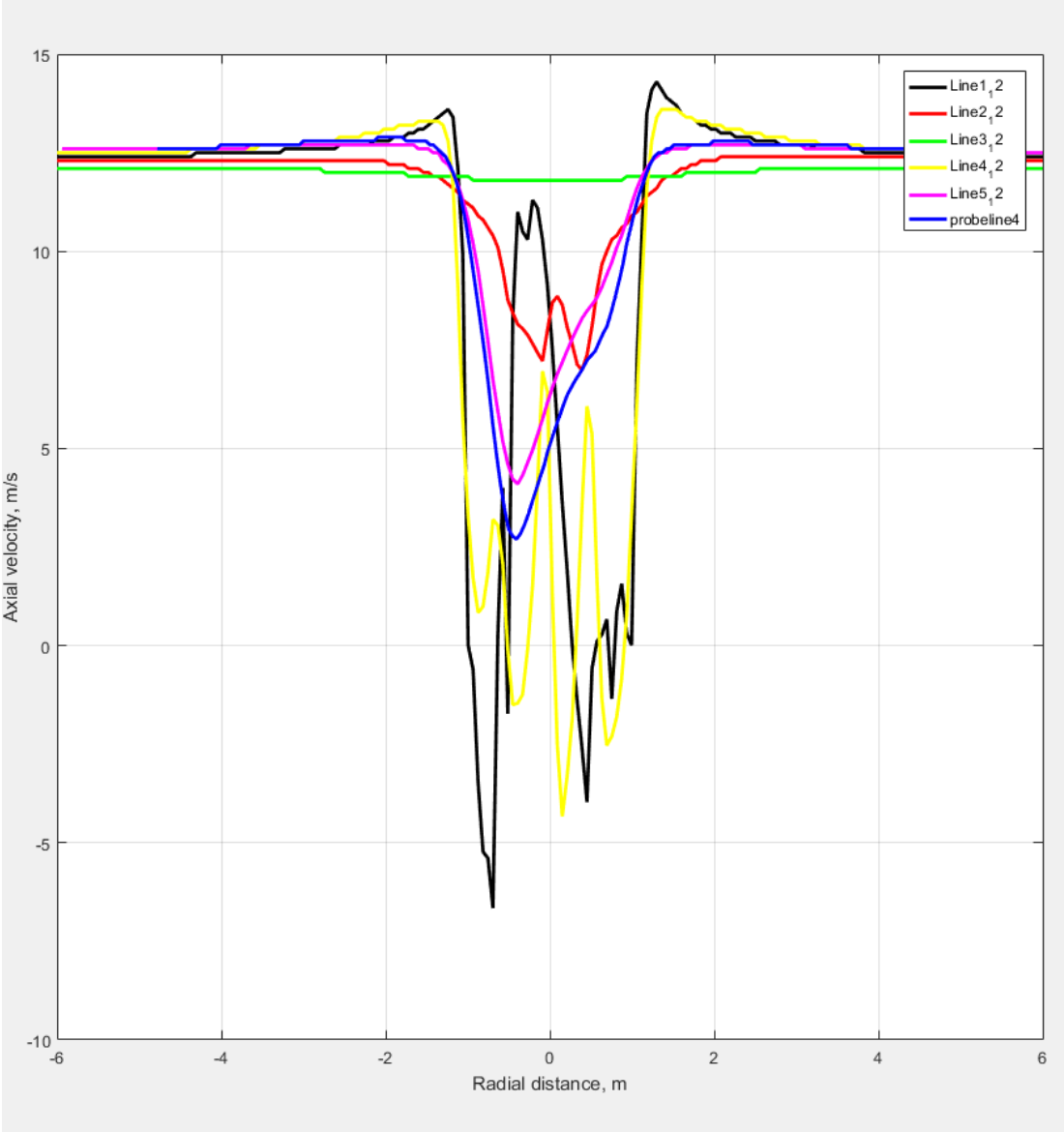

Figure 38: Axial velocity 12m/s as a function of Radial Distance

Figure 38 depicts the axial velocity as a function of radial distance for 12m/s. Line 3 shows that the upstream velocity 12m/s is not affected and the flow velocity remains constant. Line 2 presents the axial velocity at the windward of the turbine and the two valleys signify that the air is entering the VAWT. Line 1 depicts the flow phenomena at the centre of the VAWT with large peaks and valleys that represent high turbulence in the fluid passing through VAWT. Line 4 depicts the flow exiting the turbine where it carries the highest peaks and valleys. Line 5 describes the flow at the leeward 4m away from the turbine. It can be seen that the strongest deficits were found at the leeward of the turbine due to shear and high turbulence generation.

Case Study 4 (16m/s)

In this simulation, 16m/s has been used as the inlet velocity. Similarly, case studies 1, 2 and 3 Figure 39 represents an x-y projected area of the flow in u direction. It depicts the wake region at 5% more than the inlet free stream velocity (16m/s). Using Iso-surface tool from post-process, the maximum distance can be probed to be 4.7m. As in case studies 1, 2 and 3 it can be clearly identified that the wake region at the right of the VAWT forms longer wake effect, this should be taken in consideration when measuring the maximum distance in the Y direction. It can be concluded that the maximum distance required to place another VAWT is 9.4m.

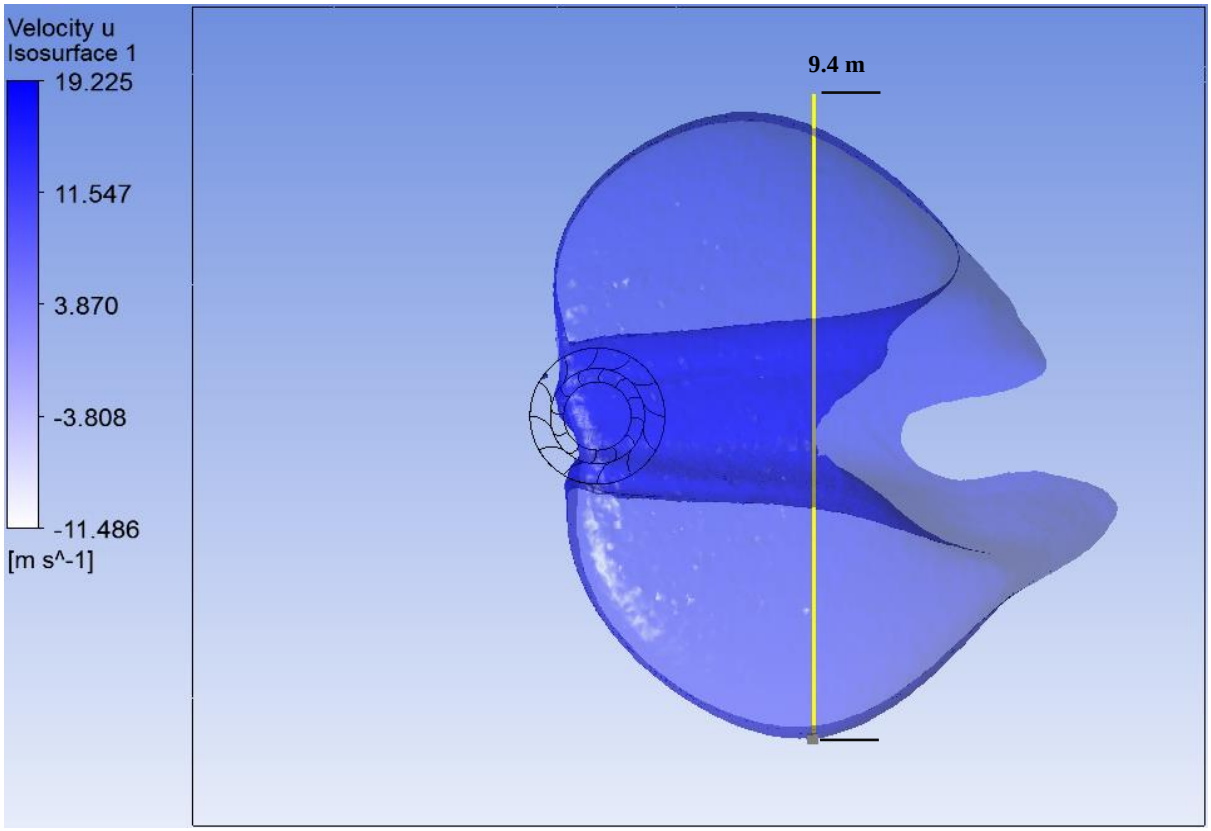

Figure 39: Spatial distribution of velocity set at 5% more than the inlet velocity (16m/s)

Comparing Figure 39 to Figure 36, Figure 30 and Figure 33 it can be clearly identified that the maximum distance probed is decreased when measured at 5% more than the inlet velocity. The maximum distance measured at Figure 39 for 5% more than the inlet velocity 16m/s is 9.4m any turbine placed inside the wake region will be affected by the neighbouring turbine and will not operate under normal wind conditions.

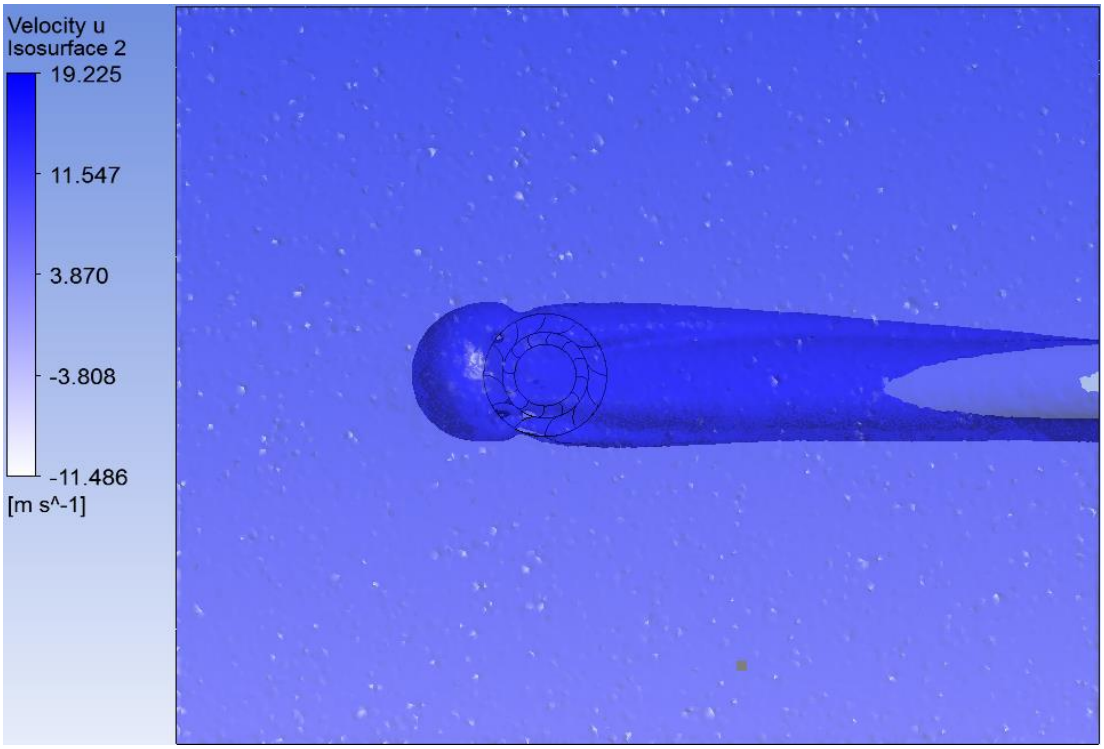

(a) Top view

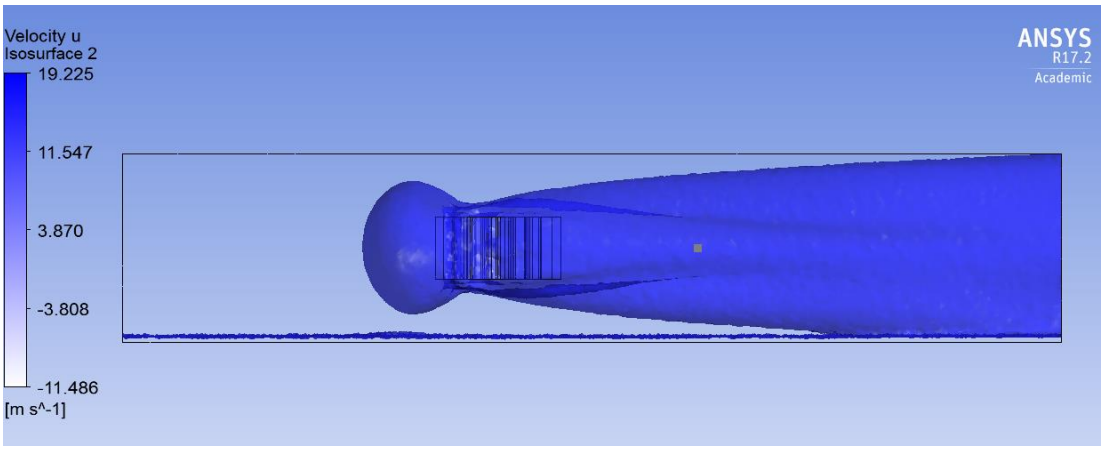

(b) Side view

Figure 40: Spatial distribution of velocity set at 5% less than the inlet velocity (16m/s)

Figure 40 (a) depicts a top view of the wake region 5% less than the inlet velocity (16m/s) and Figure 40 (b) depicts the side view of 5% less than the inlet velocity 16m/s. It represents the flow formation in z-x cross section. From this figure, it can be clearly seen that the inlet is distant from the pressure zone surrounding the VAWT. It can also be seen that the free stream velocity 16m/s is decreased around the VAWT region due to the VAWT that acts like an obstruction. As in Figure 31, Figure 34 and Figure 37; the velocity at the leeward of the VAWT is highly affected and a wake is formed as shown in Figure 40 (a) (b). The wake forms the same shape as in Figure 31, Figure 34 and Figure 37 although the operating speeds differ.

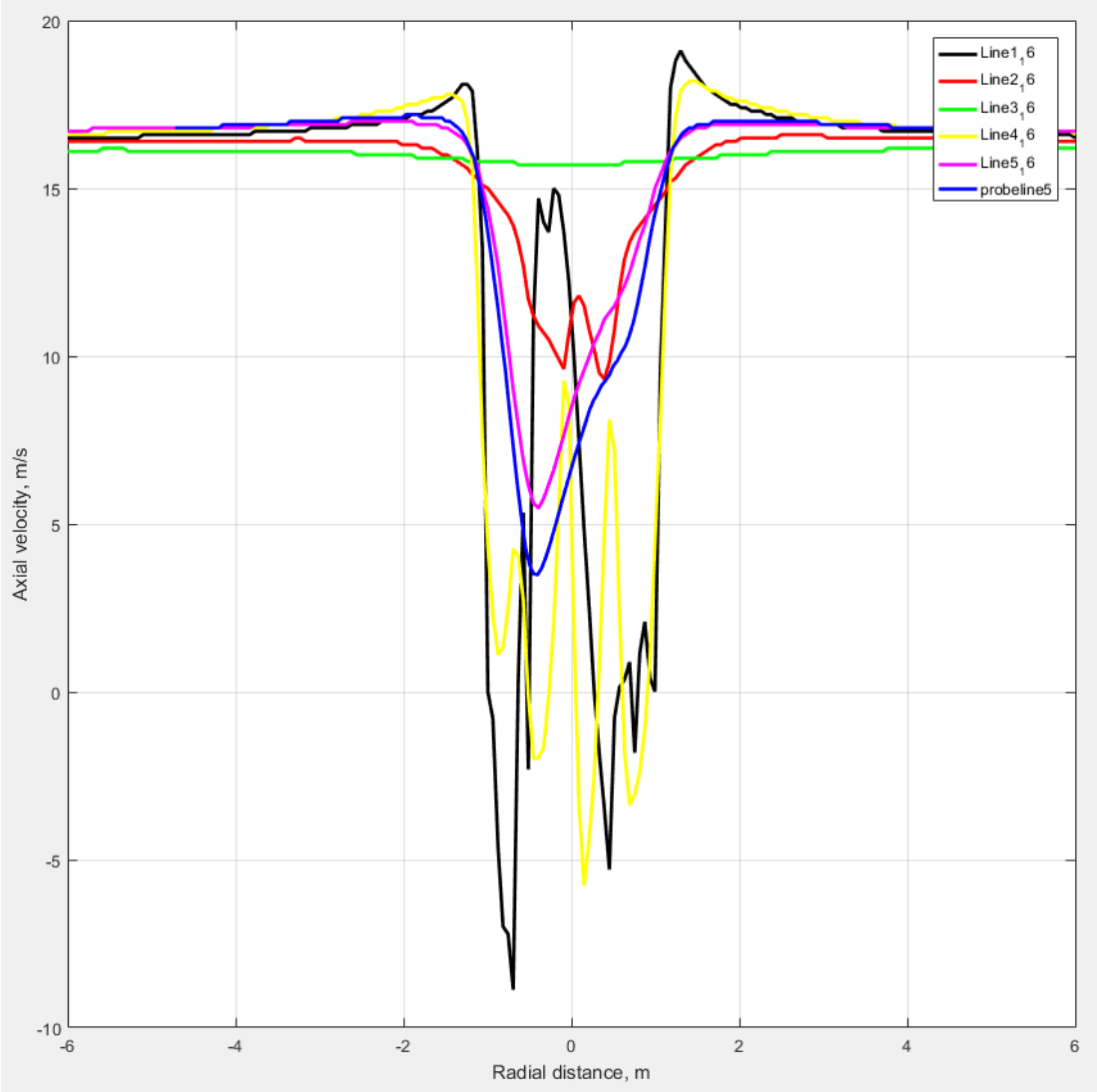

Figure 41: Axial velocity 16m/s as a function of Radial Distance

Figure 41 depicts the axial velocity as a function of radial distance for 16m/s. Line 3 shows that the upstream velocity 16m/s is not affected and the flow velocity remains constant. Line 2 presents the axial velocity at the windward of the turbine and the two peak and valleys signify that the air is entering the VAWT. Line 1 depicts the flow phenomena at the centre of the VAWT; this line shows the steepest peak and valleys due to circulations of the fluid particles. Line 4 depicts the flow exiting the turbine where it carries the highest peaks and valleys. Line 5 describes the flow at the leeward 4m away from the turbine. It can be seen that the strongest deficits were found at the leeward of the turbine due to shear and high turbulence generation.

Case Study 5 (20m/s)

In this simulation, 20m/s has been used as the inlet velocity. Similarly, as in Case 1, 2, 3 and 4 Figure 42 represents the x-y projected area of the flow in u direction. It depicts the wake region at 5% more than the inlet free stream velocity (21m/s). Using Iso-surface tool from post-process, the maximum distance can be probed to be 4.7m. As in Case Study 1, 2, 3 and 4 it can be clearly identified that the wake region at the right of the VAWT forms longer wake effect, this should be taken in consideration when measuring the maximum distance in the Y direction. It can be concluded that the maximum distance required to place another VAWT is 9.4m.

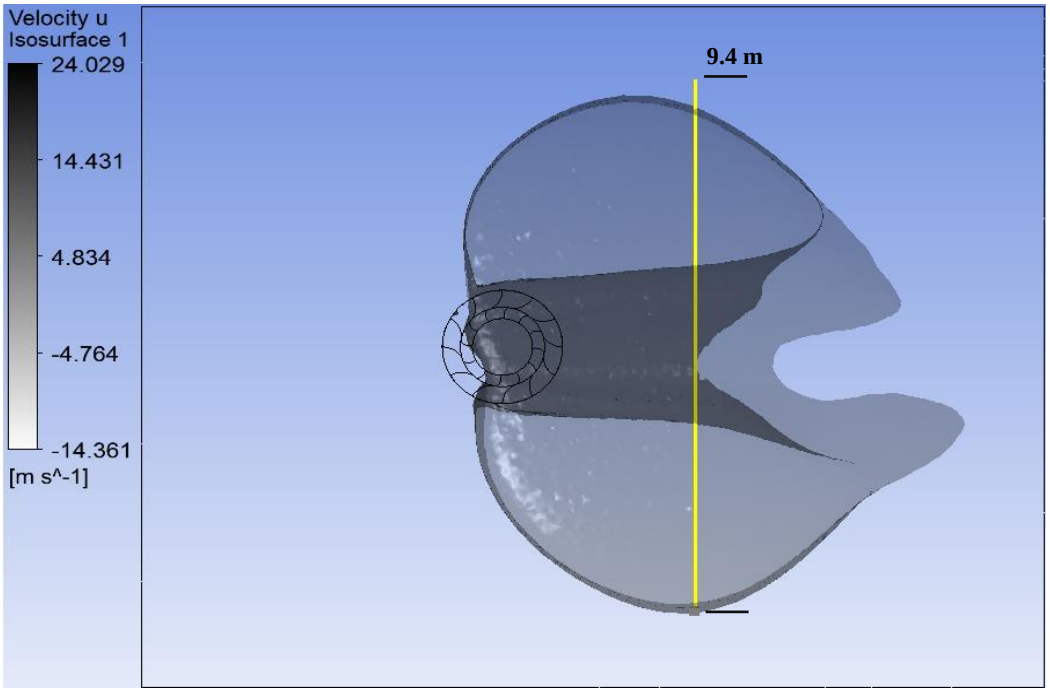

Figure 42: Spatial distribution of velocity set at 5% more than the inlet velocity (20m/s)

Comparing Figure 42 to Figure 39, Figure 36, Figure 33 and Figure 30 it can be clearly recognised that the maximum distance probed is decreased when measured at 5% more than the inlet velocity. The maximum distance measured at Figure 42 for 5% more than the inlet velocity 20m/s is 9.4m any turbine placed inside the wake region will be affected by the neighbouring turbine and will not operate under normal wind conditions.

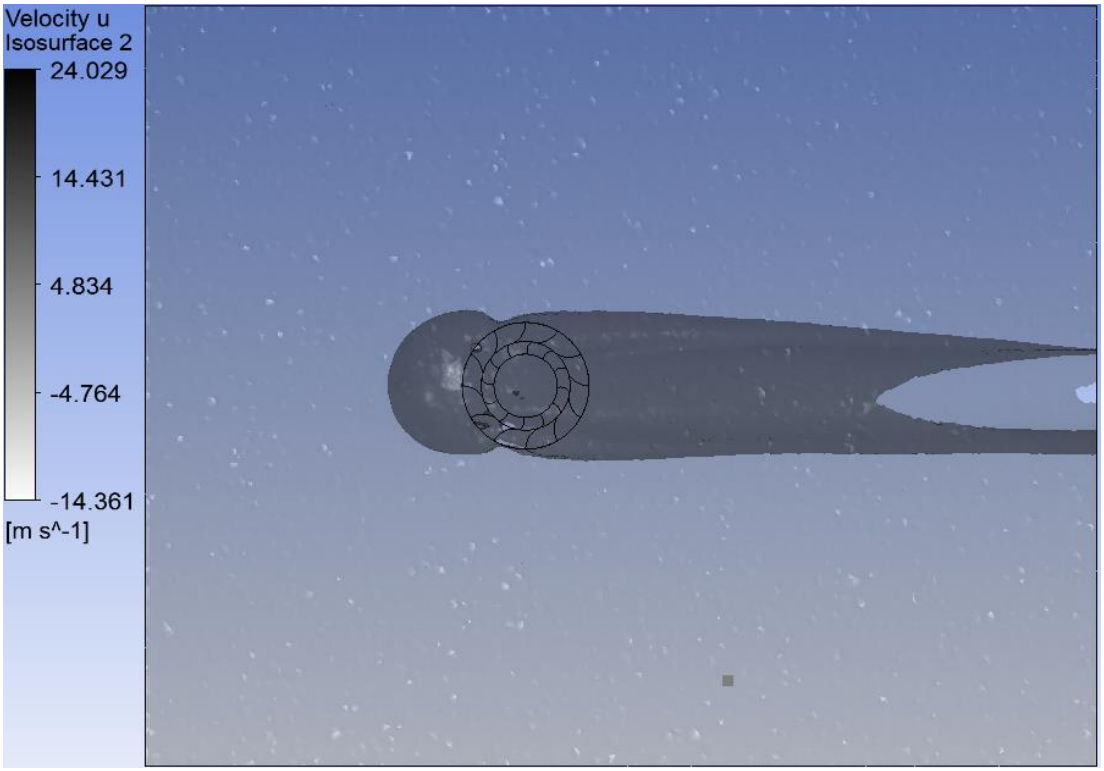

(a) Top view

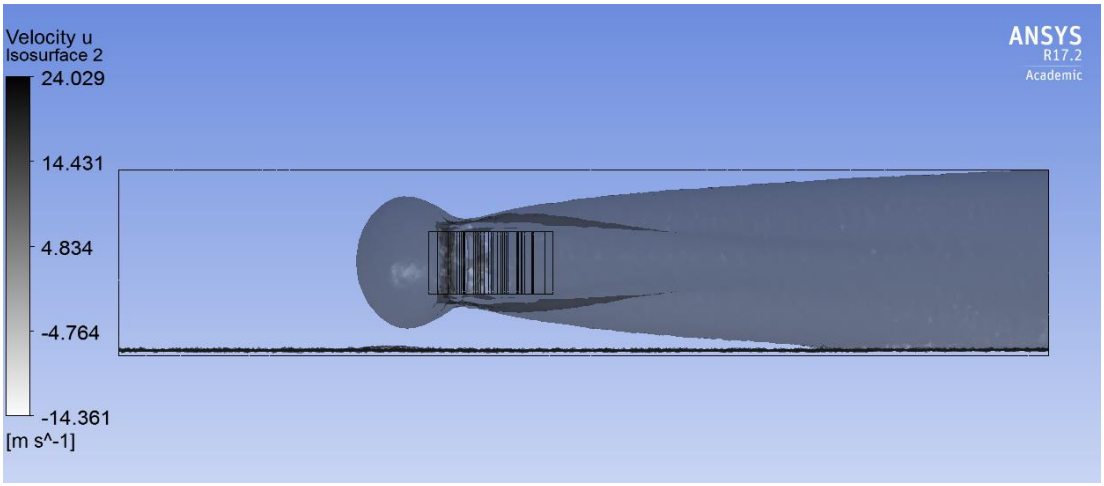

(a) Side view

Figure 43: Spatial distribution of velocity set at 5% less than the inlet velocity (20m/s)

Figure 43 (a) depicts a top view of the wake region 5% less than the inlet velocity (20m/s) and Figure 43 (b) depicts the side view of 5% less than the inlet velocity 20m/s. It represents the flow formation in z-x cross section. From this figure, it can be clearly seen that the inlet is distant from the pressure zone surrounding the VAWT. It can also be seen that the free stream velocity 20m/s is decreased around the VAWT region due to the VAWT that acts like an obstruction. As in Figure 31, Figure 34, Figure 37 and Figure 40; the velocity at the leeward of the VAWT is highly affected and a wake is formed as shown in Figure 43 (a) (b). The wake

forms the same shape as in Figure 31, Figure 34, Figure 37 and Figure 40 although the operating speeds differ.

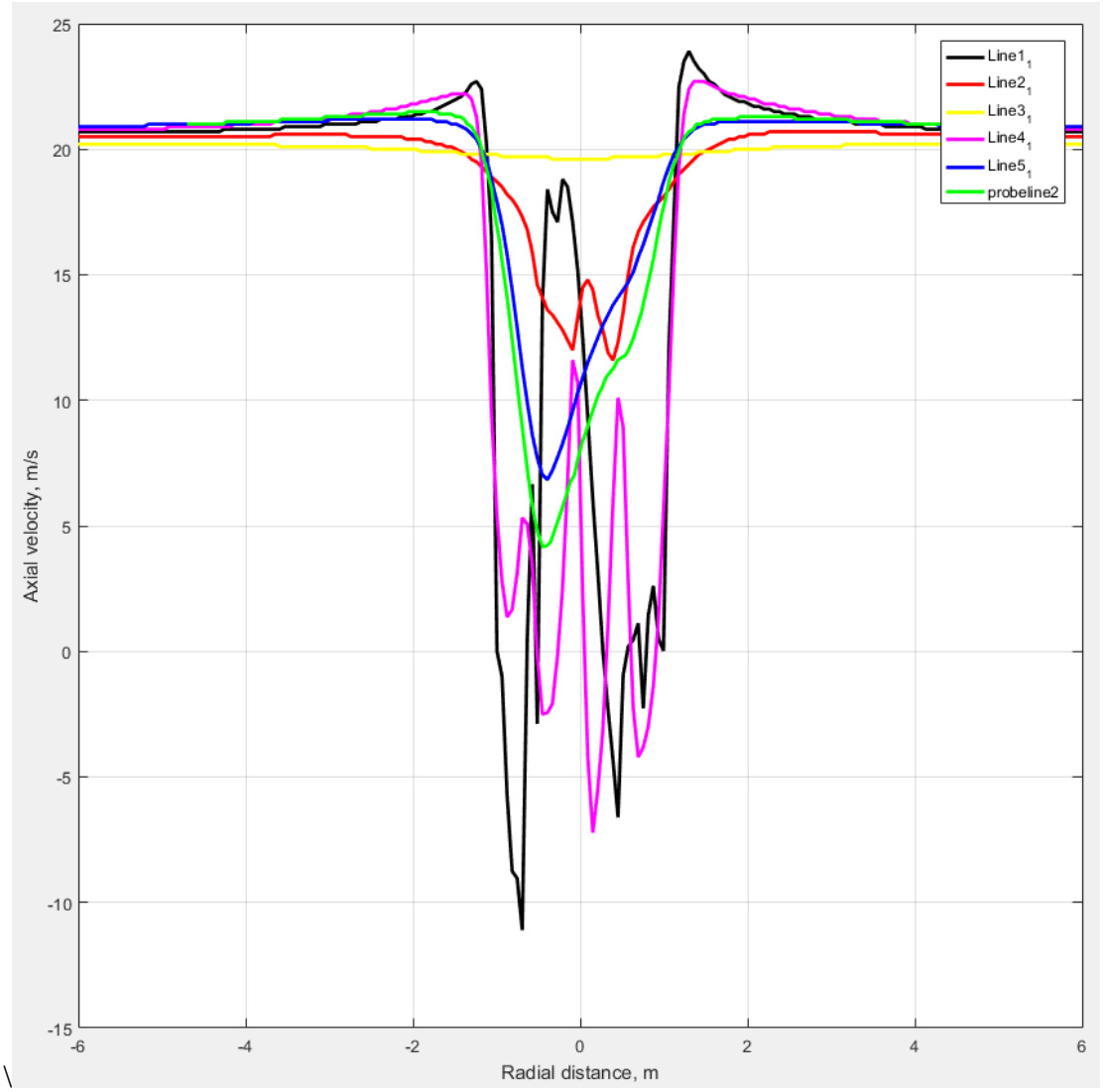

Figure 44: Axial velocity 20m/s as a function of Radial Distance

Figure 44 depicts the axial velocity as a function of radial distance for 20m/s. Line 3 shows that the upstream velocity 20m/s is not affected and the flow velocity remains constant. Line 2 presents the axial velocity at the windward of the turbine and the two peak and valleys signify that the air is entering the VAWT. Line 1 depicts the flow phenomena at the centre of the VAWT; this line shows the steepest peak and valleys due to circulations of the fluid particles. Line 4 depicts the flow exiting the turbine where it carries the highest peaks and valleys. Line 5 describes the flow at the leeward 4m away from the turbine. It can be seen that the strongest deficits were found at the leeward of the turbine due to shear and high turbulence generation.

4.5. MATHEMATICAL TOOL ANALYSIS

Table 12 summarise the various velocities that have been studied in this research. It provides the distance required between two VAWT for each flow velocity. It can be seen that 4m/s wind velocity requires 5.0 m of inter-turbine spacing to achieve ultimate power production. It can be seen from Table 12 the actual distance 5.0m in case study 1 has been multiplied into safety factor of 2 due to computational errors and to avoid wake interference. It can also be seen that increasing the wind velocity will result in decreasing the inter-turbine spacing as seen in case studies 2, 3, 4 and 5. Therefore, it can be concluded that 10m is an optimal inter-turbine distance that is insensitive to wind speed for VAWT's when placed side by side on a wind farm.

Case Study	Velocity (m/s)	Distance (m)	Distance x 2 (m)
1	4	5.02	10.04
2	8	4.9	9.8
3	12	4.8	9.6
4	16	4.7	9.4
5	20	4.7	9.4

Table 12: Maximum distance required for various inlet velocities

Figure 45 shows that velocities above 20m/s require less inter-turbine spacing, where a novel distance mathematical model has been optimized.

L=-0.0389v+10.098 Equation 11

Where L is the optimal distance required to place another vertical axis wind turbine and v is flow stream wind velocity.

Hence, Equation 11 can be used to predict the optimal distance for VAWT operating in an urban environment with realistic accuracy.

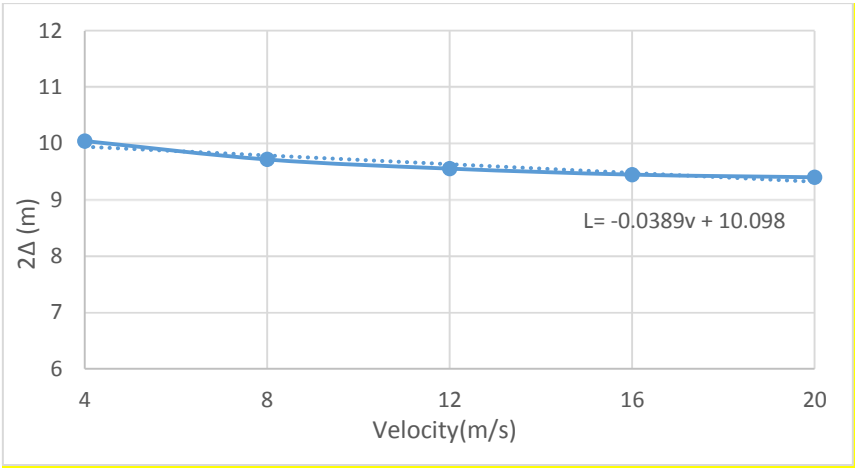

Figure 45: VAWT Velocity as a function of Optimal Distance

Chapter 5
Conclusions

The following chapter provides a brief summary of the research synopsis along with the research aims and objectives. It also summarises the major achievements of the literature, researchers and engineers. Future recommendations for further work is also proposed in this chapter.

5.1. RESEARCH PROBLEM SYNOPSIS

The need to identify the distance between the vertical axis wind turbines is a significant parameter for designers to improve the performance of the VAWT which will result in maximum power production, less installation costs and minimal land area.

Although many researchers have studied the arrangement of the HAWT and VAWT, some limitations to the studies conducted have been found. In order to accurately predict the distance required to place side by side VAWT under transient flow conditions should have been considered, in addition to associating it to an urban environment where there will be various obstructions such as buildings and trees. To overcome the limitations found in the existing literature, numerical analysis was carried out.

To accurately anticipate the distance required to place VAWT's linearly under various flow velocities, detailed aim and objectives were formulated, which are all defined clearly in the scope of this research. A summary of the aim with the main achievements of this study is detailed below.

It can be concluded that the approach of using computational fluid dynamics tool is effective, where the flow behaviour around the vertical axis wind turbine can be clearly visualised under various flow velocities and operating conditions.

5.2. RESEARCH AIMS AND MAJOR ACHIEVEMENTS

The aim of this study has been defined after conducting an extensive search in the literature to identify the gaps within the literature. The research aim is to develop a prediction model to establish the optimal distance between VAWT's and to investigate the effect of distance on various operating speed (4m/s-20m/s).

Achievement # 1: This study provides a numerical analysis of the flow field around a single vertical axis wind turbine under transient conditions. The velocity field was investigated in the radial direction so that the flow distribution in the vicinity can be identified. This study analysed five cases of inlet velocity 4m/s, 8m/s, 12m/s, 16m/s and 20m/s in order to predict the major distance required to place side by side VAWT's in a wind farm.

Achievement # 2: A novel prediction model that forecast the distance by implementing wind speed was obtained. Where VAWT's designers can benefit from the prediction model attained in this study, as the model can initially predict the distance of any wind speed. This study

verified that CFD can also be an effective tool in estimating optimal distance by measurement of maximum wake region.

5.3. THESIS CONCLUSIONS

A complete detailed study regarding distance optimisation of vertical axis wind turbines operating in a sustainable urban environment has been carried out, to support the gap found in the existing literature and to add a novel prediction tool to improve the design layout of wind farms. It has been analysed that within the expected operating range (4m/s-20m/s) the distance is independent of the wind speed. The significant conclusions from every objective of this research are summarised as follows:

Research objective # 1: To investigate the flow phenomenon around a single vertical axis wind turbine.

The numerical based investigation has been carried out to investigate the flow in the vicinity around a single VAWT operating under transient conditions. The maximum wake region has been found at 5% more from the free stream velocity. It has also been observed that high wind velocity requires less distance when placing side by side vertical axis wind turbines.

Research objective # 2: Determine the maximum distance required for positioning multiple vertical axis wind turbine without wake interference during various wind speeds.

After conducting detailed flow analysis, the axial velocity (u) around the VAWT was analyzed using post process. It was found that the wake retains its maximum shape at a velocity 5% more than the inlet velocity. This is due to the rotation of the rotor blades with respect to the stator blade which causes the flow velocity to increase or reduce. Hence, it leads to the generation of large wakes which occupy the vicinity, and which should be taken into consideration when placing another VAWT to avoid wake interference, as it will result in decreasing the performance of VAWT. Therefore, the optimal distance measured was at 5% more than the free stream velocity, as this velocity will avoid wake interference when considering a number of vertical axis wind turbines operating side by side linearly.

Research objective # 3: Develop a mathematical tool that is used to determine the maximum distance for VAWT position in a linear arrangement.

Considering the distances obtained from objective two, a novel distance prediction model has been developed using numerical tools. It has been noticed that the level of accuracy of the mathematical model is highly accurate.

5.4. RECOMMENDATIONS FOR FUTURE WORK

Distance optimisation of the vertical axis wind turbine operating under various wind velocities has been examined in the current study, where the gap identified in the literature is filled. However, this study revealed areas that require further research in increasing the overall performance of VAWT's. The main areas recognised for further research are explained below:

Recommendation # 1

Applying the novel distance predication model to accurately model a vertical axis wind turbine using various wind farm arrangements in order to further analyse the wake. This will require enormous computational power and time but it will provide the researchers with the overall power produced.

Recommendation # 2

In the present study, it became clear that errors could arise in the VAWT model due to a lack of consideration the actual thickness of the rotor and stator blades. These errors can be reduced by designing a vertical axis wind turbine model utilizing CAD software and after that, integrating the model to CFD.

Recommendation # 3

The exponential growth in Additive Manufacturing (AM) Technology is being utilised effectively in various research areas including VAWT. Bassett et al. [38] conducted research on Fused Material Deposition techniques to manufacture VAWT for disaster relief and rural electrification. Also, Guerrero-Villar et al. [39] conducted research on the development of wind turbines using prototypes generated from FDM. Therefore, it will be helpful in producing commercially viable scale models of VAWT turbines in order to enhance their efficiency.

Recommendation # 4

More parameters can be investigated using this model such as two directional spacing between VAWT's, different arrangements of VAWT's on the farm field, vertical consideration related to the urban environment, proximity of buildings and considerably more.

REFERENCES

[1] F. Mohamed, "Optimal Design of A Vertical Axis Wind Turbine for Urban Environment," Huddersfield, 2015.

[2] A. Y. Hassan and D. R. Hil, Islamic Technology: An illustrated History, Cambridge: Cambridge University Press, 1986.

[3] D. Spera, Wind Turbine Technology: Fundamental Concepts of Wind Turbine Engineering, New York: ASME Press, 1994.

[4] British Wind Energy Association, Wind energy for the Eighties, Stevenage: Peter Peregrinus, 1982.

[5] W. Leithead, "Wind Energy," *Philosophical Transactions of the Royal Society A: Mathematical, Physical and Engineering Sciences,* vol. 365, no. 1853, pp. 957-970, 2007.

[6] J. Mann, J. N. Sørensen and P.-E. Morthorst, "Wind Energy," *ENVIRONMENTAL RESEARCH LETTERS,* vol. 3, no. 1, p. 5001, 2008.

[7] J. Bremseth and K. Duraisamy, "Computational analysis of vertical axis wind turbine arrays," *Theoretical and Computational Fluid Dynamics,* vol. 30, no. 5, pp. 387-401, 2016.

[8] N. Nixon, "Timeline: The history of wind power," The Gaurdian, 2008.

[9] Energy Dept. Reports, "U.S. Wind Energy Production and Manufacturing Reaches Record Highs," U.S. Department of Energy, 2013.

[10] R. Saidur, K. Islam, N. Rahim and K. Solangi, "A review on global wind energy policy," *Renewable and Sustainable Energy Reviews,* vol. 14, pp. 1744-1762, 2010.

[11] U. Büsgen and W. Dürrschmidt, "The expansion of electricity generation from renewable energies in Germany: A review based on the Renewable Energy Sources Act Progress Report 2007 and the new German feed-in legislation," *Energy Policy,* vol. 37, no. 7, pp. 2536-2545, 2009.

[12] G. Herbert, S. Iniyan, E. Sreevalsan and S. Rajapandian, "A review of wind energy technologies," *Renewable and Sustainable Energy Reviews,* vol. 11, no. 6, pp. 1117-1145, 2007.

[13] M. Islam, S. Mekhilef and R. Saidur, "Progress and recent trends of wind energy technology," *Renewable and Sustainable Energy Reviews,* vol. 21, pp. 456-468, 2013.

[14] M. Jafaryar, R. Kamrani, M. Gorji-Bandpy, M. Hatami and D. Ganji, "Numerical optimization of the asymmetric blades mounted on a vertical axis cross-flow wind turbine," *International Communications in Heat and Mass Transfer,* vol. 70, pp. 93-104, 2016.

[15] G. Colley, R. Mishra, V. Rao and R. Woolhead, "Effect of rotor blade position on Vertical Axis Wind Turbine performance," in *Proceedings of the International Conference on Renewable Energies and Power Quality* , Granada (Spain), 2010.

[16] L. Danao, J. Edwards, O. Eboibi and R. Howell, "The Performance of a Vertical Axis Wind," in *Proceedings of the World Congress on Engineering,* London, 2013.

[17] A. P. Schaffarczyk, "Types of Wind Turbines," in *Introduction to Wind Turbine Aerodynamics,* Springer, 2014, pp. 7-20.

[18] X. Jin, G. Zhao, K. Gao and W. Ju, "Darrieus vertical axis wind turbine: Basic research methods," *Renewable and Sustainable Energy Reviews,* vol. 42, pp. 212-225, 2015.

[19] J. González, M. Payán, J. Santos and F. González-Longatt, "A review and recent developments in the optimal wind-turbine micro-siting problem," *Renewable and Sustainable Energy Reviews,* vol. 30, pp. 133-144, February 2014.

[20] F. Cassola, M. Burlando, M. Antonelli and C. Ratto, "Optimization of the Regional Spatial Distribution of Wind Power Plants to Minimize the Variability of Wind Energy Input into Power Supply Systems," *Journal of Applied Meteorology and Climatology,* vol. 47, no. 12, pp. 3099-3116, 2008.

[21] A. Clarke, "Wind farm location and environmental impact," *International Journal of Ambient Energy,* vol. 10, no. 3, pp. 129-144, 1989.

[22] T. Ramachandra and B. Shruthi, "Spatial Mapping of Renewable Energy Potential," *Renewable and Sustainable Energy Reviews,* vol. 11, no. 7, pp. 1460-1480, 2007.

[23] S. Baban and T. Parry, "Developing and applying a GIS-assisted approach to locating wind farms in the UK," *Renewable Energy,* vol. 24, no. 1, pp. 59-71, 2001.

[24] Y. Chen, H. Li, B. He, P. Wang and K. Jin, "Multi-objective genetic algorithm based innovative wind farm layout optimization method," *Energy Conversion and Management,* vol. 105, pp. 1318-1327, 2015.

[25] R. Shakoor, M. Hassan, A. Raheem and Y.-K. Wu, "Wake Effect Modeling: A Review of Wind Farm Layout Optimization using Jensen's Model," *Renewable and Sustainable Energy Reviews,* vol. 58, pp. 1048-1059, 2016.

[26] H. Lam and H. Peng, "Study of wake characteristics of a vertical axis wind turbine by two and three-dimensional computational fluid dynamics simulations," *Renewable Energy,* vol. 90, pp. 386-398, 2016.

[27] S. Zanforlin and T. Nishino, "Fluid dynamic mechanisms of enhanced power generation by closely spaced vertical axis wind turbines," *Renewable Energy,* vol. 99, pp. 1213-1226, 2016.

[28] G. Mosetti, C. Poloni and B. Diviacco, "Optimization of wind turbine positioning in large windfarms by means of a genetic algorithm," *Journal of Wind Engineering and Industrial Aerodynamics,* vol. 51, no. 1, pp. 105-116, January 1994.

[29] J. Orosa, E. García-Bustelo and A. Oliveira, "Low speed wind concentrator to improve wind farm," in *35th Annual Conference of IEEE Industrial Electronics*, 2009.

[30] A. Kusiak and A. Verma, "Monitoring Wind Farms With Performance Curves," *IEEE Transactions on Sustainable Energy,* vol. 4, no. 1, pp. 192-199, 2013.

[31] K. Park, *Optimal Design of A Micro Vertical Axis Wind Turbine for Sustainable Urban Environment,* University of Huddersfield, 2013.

[32] G. Colley, *Design, Operation and Diagonostics of a Vertical Axis Wind Turbine,* Huddersfield: University of Huddersfield, 2012.

[33] H. Versteeg and W. Malalasekera, An Introduction to Computational Fluid Dynamics: The Finite Volume Method, 2nd ed., Essex: Pearson Education Limited, 2007.

[34] F. Schmitt, ""About Boussinesq's turbulent viscosity hypothesis: historical remarks and a direct evaluation of its validity," pp. 617-627, 2007.

[35] W. T. T. Oberkampf and C. Hirsch, "Verification, Validation, and Predictive Capability in Computational Engineering and Physics," *Applied Mechanics Reviews,* vol. 57, no. 5, pp. 345-384, December 2004.

[36] G. Colley and R. Mishra, "Performance characteristics of a Vertical Axis Wind Turbine (VAWT) under transient conditions," in *n: Proceedings of the 24th International Congress on Condition Monitoring and Diagnostics Engineering Management*, Stavanger, Norway, 2011.

[37] F. R. Menter, "Two-Equation Eddy-Viscosity Turbulence Models for Engineering Applications," *AIAA*, vol. 32, no. 8, pp. 1598-1605, 1994.

[38] G. Colley and R. Mishra, "Computational flow field analysis of a Vertical Axis Wind Turbine," *Renewable Energy and Power Quality*, 2011.

[39] K. Bassett, R. Carriveau and D.-K. Ting, "3D printed wind turbines part 1: Design considerations and rapid manufacture potential," *Sustainable Energy Technologies and Assessments*, vol. 11, pp. 186-193, 2015.

[40] F. Guerrero-Villara, E. Torres-Jimeneza, R. Dorado-Vicentea and J. Jiménez-Gonzáleza, "Development of Vertical Wind Turbines via FDM Prototypes," *Procedia Engineering*, vol. 132, pp. 78-85, 2015.

[41] J. D. Anderson, Fundamentals of Aerodynamics, Tata McGraw-Hill Education, 1985.

[42] T. Asim, R. Mishra and K. Ubbi, "Effect of the Shape of Stator Blades on the Performance Output of a Vertical Axis Marine Current Turbine," 2013.

[43] H. Beri and Y. Yao, "Numerical Simulation of Unsteady Flow to Show Self-starting of Vertical Axis Wind Turbine Using Fluent," *Journal of Applied Sciences*, no. 11, pp. 962-970, 2011.

[44] M. Castelli and E. Benini, "ffect of blade thickness on darrieus vertical-axis wind turbine performance," in *2nd international conference on computer modelling and simulation*, 2011.

[45] M. Castelli, G. Grandi and E. Benini, "Numerical Analysis of Laminar to Turbulent," *International Journal of Mechanical, Aerospace, Industrial, Mechatronic and Manufacturing Engineering*, vol. 6, no. 3, 2012.

[46] C. Chapman, High Speed Flow, vol. 23, Cambridge University Press, 2000.

[47] M. Elkhoury, T. Kiwata and E. Aoun, "Experimental and numerical investigation of a three-dimensional vertical-axis wind turbine with variable-pitch," *Journal of Wind Engineering and Industrial Aerodynamics*, vol. 139, pp. 111-123, April 2015.

[48] S. Ghatage and J. Joshi, "Optimisation of Vertical Axis Wind Turbine: CFD Simulations and Experimental Measurements," *The Canadian Journal of Chemical Engineering*, vol. 90, no. 5, pp. 1186-1201, 2012.

[49] S. Heier, Grid Integration of Wind Energy, 3rd ed., John Wiley & Sons, 2014.

[50] Y. Hu, T. Tong and S. Wang, "A New Type of VAWT and Blade Optimization," in *International Technology and Innovation Conference*, Xian, China, 2009.

[51] A. Kusiak, H. Zheng and Z. Song, "Models for monitoring wind farm power," *Renewable Energy,* vol. 34, no. 3, pp. 583-590, March 2009.

[52] S. C. McIntosh, H. Babinsky and T. Bertényi, "Optimizing the Energy Output of Vertical Axis Wind," in *45th AIAA Aerospace Sciences Meeting and Exhibit*, Renop, Nevada, 2007.

[53] S. C. McIntosh, H. Babinsky and T. Bertényi, "Unsteady Power Output of Vertical Axis Wind Turbines Operating within a Fluctuating Free-Stream," in *46th AIAA Aerospace Sciences Meeting and Exhibit*, Reno, Nevada, 2008.

[54] M. Mohamed, "Performance investigation of H-rotor Darrieus turbine with new airfoil shapes," *Energy,* vol. 47, no. 1, pp. 522-530, 2012.

[55] K. Pope, G. Naterer, I. Dincer and E. Tsang, "Power correlation for vertical axis wind turbines with varying geometries," *International Journal of Energy Research,* vol. 35, no. 5, pp. 423-435, 20 April 2010.

[56] E. Rareshide, A. Tindal, C. Johnson, A. Graves, E. Simpson, J. Bleeg, T. Harris and D. Schoborg, "Effects of Complex Wind Regimes on Turbine Performance," in *AWEA WINDPOWER Conference*, Chicago, 2009.

[57] F. Scheurich and R. Brown, "Modelling the aerodynamics of vertical-axis wind turbines in unsteady wind conditions," *Wind Energy,* vol. 16, no. 1, pp. 91-107, January 2013.

[58] Z. Yuyi, L. Liang, T. Wenbin and L. Jun, "The Design of Vertical Axis Wind Turbine Rotor for Antarctic," *Information Technology Journal,* vol. 12, no. 4, pp. 604-613, 2013.

[59] A. Shahzad, T. Asim, R. Mishra and A. Paris, "Performance of a Vertical Axis Wind Turbine under Accelerating," *Procedia CIRP,* vol. 11, pp. 311-316, 2013.

[60] A. Shires and V. Kourkoulis, "Application of Circulation Controlled Blades for Vertical Axis," *Energies,* vol. 6, no. 8, pp. 3744-3763, 2013.

[61] H. Peng and H. Lam, "Turbulence effects on the wake characteristics and aerodynamic performance of a straight-bladed vertical axis wind turbine by wind tunnel tests and large eddy simulations," *Energy,* vol. 109, pp. 557-568, 2016.

[62] G. Tescione, D. Ragni, C. He, C. S. Ferreira and G. van Bussel, "Near wake flow analysis of a vertical axis wind turbine by stereoscopic particle image velocimetry," *Renewable Energy,* vol. 70, pp. 47-61, 2014.

[63] N. Choi, S. H. Nam, J. Jeong and K. Kim, "CFD Study on Aerodynamic Power Output Changes with Inter-Turbine Spacing Variation for a 6 MW Offshore Wind Farm," *Energies,* vol. 7, pp. 7483-7498, 2014.

[64] M. Avila, A. Folch, G. Houzeaux, B. Eguzkitza, L. Prieto and D. Cabez´on, "A Parallel CFD Model for Wind Farms," *Procedia Computer Science,* vol. 18, pp. 2157-2166, 2013.

[65] J. Herp, U. Poulsen and M. Greiner, "Wind Farm Power Optimization Including Flow Variability," *Renewable Energy,* vol. 81, pp. 1733-181, 2015.